© 2015. Published by The Company of Biologists Ltd | Development (2015) 142, 486-496 doi:10.1242/dev.108266

RESEARCH ARTICLE

Regulation of ECM degradation and axon guidance by growth cone invadosomes

Miguel Santiago-Medina, Kelly A. Gregus, Robert H. Nichol, Sean M. O'Toole and Timothy M. Gomez*

ABSTRACT

Invadopodia and podosomes, collectively referred to as invadosomes, are F-actin-rich basal protrusions of cells that provide sites of attachment to and degradation of the extracellular matrix. Invadosomes promote the invasion of cells, ranging from metastatic cancer cells to immune cells, into tissue. Here, we show that neuronal growth cones form protrusions that share molecular, structural and functional characteristics of invadosomes. Growth cones from all neuron types and species examined, including a variety of human neurons, form invadosomes both *in vitro* and *in vivo*. Growth cone invadosomes contain dynamic F-actin and several actin regulatory proteins, as well as Tks5 and matrix metalloproteinases, which locally degrade the matrix. When viewed using three-dimensional super-resolution microscopy, F-actin foci often extended together with microtubules within orthogonal protrusions emanating from the growth cone central domain. Finally, inhibiting the function of Tks5 both reduced matrix degradation *in vitro* and disrupted motoneuron axons from exiting the spinal cord and extending into the periphery. Taken together, our results suggest that growth cones use invadosomes to target protease activity during axon guidance through tissues.

KEY WORDS: Axon guidance, Pathfinding, Neural development, *Xenopus*

INTRODUCTION

During development, growth cones guide neurites to their proper synaptic partners by functioning as highly specialized molecular sensors. Receptors on the surface of growth cones detect the molecular constitution of the surrounding extracellular matrix (ECM) and the secreted protein gradients in the environment (Kolodkin and Tessier-Lavigne, 2011). Receptor engagement elicits adhesion and intracellular signaling cascades that affect growth cone motility (Lowery and Van Vactor, 2009). Integrated cell signals converge onto the actomyosin and microtubule (MT) cytoskeletons, which power the force-generating machinery responsible for growth cone motility and axon guidance (Dent et al., 2011).

Growth cones contain many structural projections that rearrange in response to guidance cues. Growth cones are also compartmentalized into specialized regions where the cytoskeleton is differentially organized. Within the peripheral domain, F-actin is organized into bundles and a dense meshwork array that generate protrusive filopodia and lamellipodia. Towards the rear of the growth cone is the central domain where stable, bundled MTs splay from the axon shaft. Lastly, the transition zone exists at the interface between the peripheral and central domains (P- and C-domains, respectively), and is a region of strong actomyosin contraction and F-actin depolymerization (Medeiros et al., 2006).

In two-dimensional environments, growth cones use filopodia to help direct neurite extension upon planar substrata. However, growth cones *in vivo* must penetrate and transverse tissues, and detect secreted guidance cues from sources deep within the embryo. To direct guidance through three-dimensional (3D) environments, growth cones may form protrusions on their apical and basal surfaces, reminiscent of podosomes and invadopodia of immune and metastatic cancer cells, respectively (Linder et al., 2011; Murphy and Courtneidge, 2011). Podosomes and invadopodia, collectively referred to as invadosomes, are filopodia-like protrusions that are associated with ECM adhesion and remodeling. Although growth cones are known to secrete matrix metalloproteinases (MMPs) during axon guidance (McFarlane, 2003; Yong et al., 2001), they have not been shown to form invadosomes.

In this study, we show that growth cones form stable, F-actin-rich puncta that are reminiscent of invadosomes of invasive cells (Murphy and Courtneidge, 2011; Murphy et al., 2011). F-actin foci form primarily within the C-domain of growth cones and colocalize with numerous invadosomal markers, such as cortactin (Cttn), active Src and Tks5. Growth cones of varied neuron types across species form invadosomes on many different substrata, as well as in the intact spinal cord, suggesting that they are a fundamental subcellular specialization of developing neurons. Growth cone invadosomes are more stable than point contact (PC) adhesions (Gomez et al., 1996; Renaudin et al., 1999), yet colocalize with several actin polymerization and bundling proteins. Consistently, growth cone invadosomes are sites of rapid F-actin turnover with concentrated free F-actin barbed ends, as well as monomeric actin. Super resolution 3D microscopy shows that the F-actin within invadosomes is oriented as a vertical column that spans the C-domain in the *z*-plane and that F-actin can extend as orthogonal 3D-protrusions from the C-domain of growth cones. Moreover, in 3D collagen gels and *in vivo*, similar projections occur from the apical and basal surfaces of growth cones. Using fluorescent gelatin, we show that growth cone invadosomes target proteolytic activity in a Tks5-dependent manner. Lastly, inhibiting invadosome targeting of MMP activity with dominant-negative Tks5 prevents proper extension of motoneuron axons into the periphery. From these findings, we have identified novel structural components of growth cones that are analogous to the invadosomes of invasive cells and are crucial in guiding axons throughout tissues of the developing nervous system.

RESULTS

F-actin foci are prominent subcellular structures within the central domain of growth cones in culture and in the intact spinal cord

When we imaged actin in fixed growth cones by using total internal reflection fluorescence (TIRF) or confocal microscopy, we observed prominent F-actin foci within the C-domain (Fig. 1), which was

Department of Neuroscience and Neuroscience Training Program, University of Wisconsin, Madison, WI 53706, USA.

*Author for correspondence (tmgomez@wisc.edu)

Received 23 January 2014; Accepted 30 November 2014

Development (2015) 142, 486-496 doi:10.1242/dev.108266

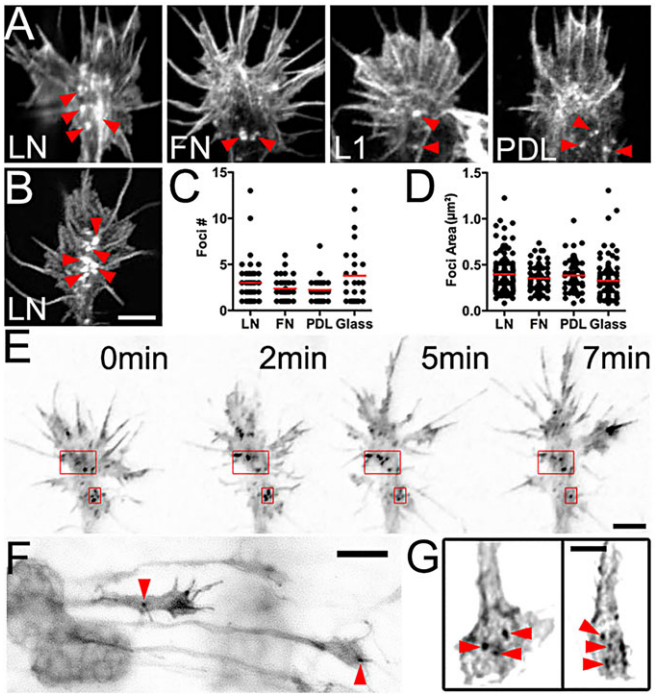

Fig. 1. Growth cones contain F-actin-rich foci within their central domain *in vitro* and *in vivo*. (A,B) Confocal images of phalloidin-labeled spinal neuron (A) or retinal ganglion cell (B) growth cones with F-actin foci (arrowheads) cultured on different substrata. (C,D). Quantification of foci number (C; $n \geq 26$) and area (D; $n \geq 51$) in growth cones on different substrata. Lines represent the mean intensity. (E) TIRF images of a live spinal growth cone on laminin expressing GFP-β-actin. Note stable F-actin foci in the C-domain as the growth cone advances (red boxes). (F,G) Confocal *z*-series projections of whole-mount *Xenopus* spinal cords with F-actin-labeled motoneurons and commissural interneurons by using targeted expression of mCh-UtrCH. (F) Lateral view shows motoneuron axons extending along the ventral fascicle with F-actin foci (arrowheads). (G) Ventral view of a spinal cord showing commissural interneuron growth cones at the midline. Scale bars: 5 μm (A,B,E,G); 10 μm (F). FN, fibronectin; LN, laminin; PDL, poly-D-lysine.

predominantly devoid of bundled F-actin. To begin to understand the role of F-actin foci in growth cones, we set out to determine whether foci formation depends on the culture substratum. For this, we cultured neurons isolated from embryonic *Xenopus* spinal cord on ECM proteins, cell adhesion molecules and non-biological substrata. We found that foci formed within the C-domain of growth cones when cultured on all of the tested substrata (Fig. 1A), including bare glass (supplementary material Fig. S1A), suggesting that these specializations do not require specific receptor engagement. To determine whether F-actin foci formed in the growth cones of diverse neuron types and across species, we cultured a variety of primary neuron types, as well as human neurons derived from induced pluripotent stem cells (iPSCs). F-actin foci formed in growth cones of all cell types tested, including human iPSC-derived neurons (Fig. 1B; supplementary material Fig. S1B-F). Although the average number (Fig. 1C) and size of F-actin foci were similar to PC adhesions (Robles and Gomez, 2006), their location in the C-domain was distinct.

To visualize F-actin in live growth cones, we expressed either β-actin fused to green fluorescent protein (GFP-β-actin) or the F-actin binding probe Utrophin-CH conjugated to mCherry (mCh-UtrCH) in neurons. High-resolution live-cell imaging showed that both GFP-β-actin and mCh-UtrCH concentrated in F-actin bundles at the growth cone leading edge, as expected, but also in prominent actin foci within the C-domain (Fig. 1E; supplementary material Fig. S2A). It is noteworthy that GFP-tagged γ-actin also targeted to actin foci when expressed in growth cones (supplementary material Fig. S2B). Time-lapse imaging showed that actin foci were relatively long-lived, with an average lifetime of 7.76±0.32 min (Fig. 1E; supplementary material Movies 1, 2), which is notably longer than that of PC adhesions (Robles and Gomez, 2006; Santiago-Medina et al., 2013). In extreme cases, actin foci were observed to form at the leading edge and remained stable until they disassembled at the rear of the growth cone (supplementary material Fig. S2C). Although the majority of foci were stable, some were motile, resembling actin comets (supplementary material Fig. S2D).

Although the growth cone morphologies observed *in vitro* appeared similar to those seen *in vivo*, it is possible that foci are only a tissue culture artifact. Therefore, to determine whether F-actin foci also formed within growth cones *in vivo*, we labeled F-actin in commissural interneurons and motoneurons with mCh-UtrCH or GFP-UtrCH, and then fixed embryos for whole-mount spinal cord imaging (see Materials and Methods). By using confocal microscopy, we observed prominent F-actin foci within motoneuron growth cones on the ventral fascicle (Fig. 1F) and commissural interneurons at the ventral midline (Fig. 1G). We conclude that growth cones of distinct neuron populations and of different species can assemble F-actin-rich foci under a variety of environmental conditions.

F-actin foci target to the basal surface of growth cones and colocalize with growth cone PC proteins, but not with classic vesicle markers

Growth cones are known to form transient PC adhesions, predominantly at the leading edge and within filopodia (Robles and Gomez, 2006) but not typically within the C-domain, where foci form and remain stable (Fig. 1). Therefore, we hypothesized that foci are not classical PC adhesions but that they might still recruit proteins implicated in integrin-dependent adhesion. To test whether F-actin foci function as adhesion sites, we immunolabeled growth cones that had been cultured on laminin for β1 integrin. We found that β1 integrin receptors targeted to F-actin foci, as well as to PC adhesions and filopodia tips (Fig. 2A). Because F-actin foci contain integrin receptors, we tested for other adhesion proteins. Paxillin (PXN) and focal adhesion kinase (FAK) both serve essential roles in PC dynamics (Myers and Gomez, 2011; Woo and Gomez, 2006), so we tested whether these adhesion proteins colocalized with F-actin foci in fixed growth cones. Immunolabeling for PXN that was phosphorylated at residue Y118 (pY118-PXN) or FAK that was phosphorylated at residue Y397 (pY397-FAK), together with F-actin, showed that adhesion proteins colocalized with a minority of F-actin foci within the C-domain (Fig. 2B-D). Next, we used two-color live-cell imaging of mCh-UtrCH with GFP-tagged PXN (PXN-GFP) to assess the dynamic assembly of F-actin foci and PC adhesions (supplementary material Movie 3). PXN-containing PC adhesions assembled at the leading edge of growth cones (Fig. 2E), which were typically devoid of F-actin foci (Fig. 2F,G). However, a majority of foci (65.7%) did emerge from pre-existing PXN PCs within the C-domain. This finding suggests that a subset of PXN-containing PC adhesions could mature into longer-lived F-actin foci that persist within the C-domain as growth cones migrate forward. By contrast, F-actin foci did not colocalize with exocytic or endocytic vesicles (supplementary material Figs S3, S4). These results suggest that F-actin foci might function as previously unidentified adhesion sites, because they

Development (2015) 142, 486-496 doi:10.1242/dev.108266

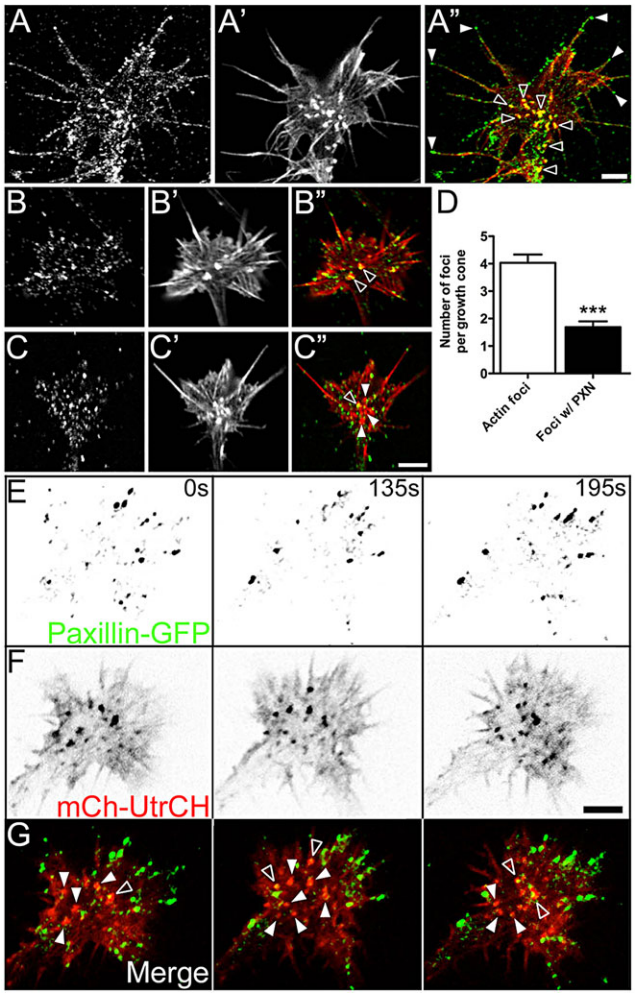

Fig. 2. F-actin foci colocalize with β1 integrin receptors and the PC proteins PXN and FAK in growth cones. (A-C) Confocal microscopy images of growth cones cultured on laminin and immunolabeled for β1 integrin (A), pY118-PXN (B) or pY397-FAK (C). (A′-C′) Phalloidin staining. (A″-C″) Merged images of immunolabeling (green) and F-actin staining (red). Note that β1 integrin targets to filopodia tips (solid arrowheads), as well as to F-actin foci (open arrowheads). Also note that pY118-PXN and pY397-FAK colocalize with some (open arrowheads), but not all, F-actin foci (solid arrowheads). (D) A minority of F-actin foci contain pY118-PXN. ***P<0.001, unpaired t-test, n=68. (E,F) Inverse contrast TIRF images of a live spinal neuron growth cone on laminin expressing both paxillin (PXN)-GFP (E) and mCh-UtrCH (F). (G) In a merged pseudo-colored image, PXN (green) colocalizes with some (open arrowheads), but not all F-actin foci (red, solid arrowheads). Scale bars: 5 µm (A,B,E-G).

form in close proximity to the substratum, remain stable and colocalize with integrins and adhesion proteins.

F-actin foci are sites of rapid actin turnover

With live-cell imaging, F-actin foci appeared as stable aggregates of F-actin, yet the dynamics of actin polymerization at foci were unclear. Moreover, some F-actin foci resembled actin comets, suggesting that rapid actin polymerization occurs at these structures. Because the process of actin polymerization requires the addition of monomeric actin (G-actin) to the barbed ends of F-actin, we tested whether actin monomers concentrated at foci. Similar to other sites of rapid actin polymerization in growth cones (Lee et al., 2013; Marsick et al., 2010), we found monomeric G-actin at F-actin foci (Fig. 3A; supplementary material Fig. S4). To determine whether foci contained uncapped barbed actin filaments for G-actin addition during actin polymerization, we used the F-actin barbed-end binding probe tetramethylrhodamine kabiramide-C (TMR-KabC) (Petchprayoon et al., 2005; Tanaka et al., 2003). TMR-KabC is a small, cell-permeable molecule that can bind to the barbed ends of F-actin and track the retrograde flow of actin filaments (Keren et al., 2008; Santiago-Medina et al., 2013, 2011). Consistent with actin polymerization at F-actin foci, TMR-KabC rapidly labeled foci in live growth cones (Fig. 3B). Note that KabC also strongly labeled F-actin filaments undergoing retrograde flow at the leading edge, which was distinct from the static labeling of actin at foci (Fig. 3C). Finally, to directly measure the rate of actin polymerization within foci, we bleached or photo-activated fluorescent protein-conjugated actin in live growth cones (supplementary material Movie 4). Either GFP-β-actin or photoactivatable-GFP (PA-GFP)-γ-actin together with mCh-UtrCH were bleached or photoactivated within foci, and the recovery rate and decay were measured, respectively (Fig. 3D-G). In fluorescence recovery after photobleaching (FRAP) experiments, the turnover rate of GFP-β-actin at foci was significantly faster compared with that of regions immediately adjacent to foci ($t_{1/2}$=6.56±0.01 s versus 8.53±0.02 s; P<0.004; Fig. 3D,E), but slower than the recovery of actin within the growth cone veil ($t_{1/2}$=5.55±0.02 s; P<0.0001). Similar rates were obtained in fluorescence decay after photoactivation (FDAP) experiments using photoactivatable-GFP at foci ($t_{1/2}$=7.11±0.01 s; Fig. 3F,G). Taken together, these data demonstrate that F-actin is highly dynamic within stable foci.

F-actin foci colocalize with key invadosome proteins

In comparison with the F-actin distribution of other cell types, growth cone F-actin foci exhibited a striking similarity to the invadosomes of immune and invasive cells. Invadosomes are long-lived actin-based protrusions located on the basal surface of cells that appear as punctate accumulations of F-actin *in vitro* (Linder et al., 2011; Murphy and Courtneidge, 2011). Invadosomes regulate cell migration by adhering to and remodeling the underlying ECM. As sites of cell adhesion, invadosomes contain integrin receptors, PXN and FAK (Chan et al., 2009). In order to begin to test the hypothesis that F-actin foci are invadosome-like protrusions of neuronal growth cones, we immunolabeled growth cones for several key invadosome markers. Cttn is a key modulator of F-actin polymerization that is necessary for invadosome formation (Kirkbride et al., 2011; MacGrath and Koleske, 2012). By using immunocytochemistry, we found that Cttn was present at the leading edge of growth cones (Fig. 4A), as has been reported previously (Decourt et al., 2009; Kurklinsky et al., 2011). However, we also found robust colocalization of Cttn with F-actin foci in the C-domain of growth cones (Fig. 4A; supplementary material Fig. S4). To confirm this distribution, we co-expressed GFP-tagged Cttn (GFP-Cttn) with mCH-UtrCH in live cells (supplementary material Movie 5). Along with Cttn, other actin regulatory proteins that have been previously implicated in invadosome formation (Murphy and Courtneidge, 2011; Philippar et al., 2008) targeted to F-actin foci, including the nucleating proteins Arp2/3 and N-WASP, the cross-linking protein α-actinin and the anti-capping factor Mena (Fig. 4B-E; supplementary material Fig. S4). Taken together, these results suggest that F-actin foci in the C-domain of growth cones represent invadosomes, which might regulate axon guidance through tissues.

One classic marker and specific modulator of invadosome formation is the adaptor protein Tks5, which is phosphorylated by Src (Courtneidge, 2012). Phosphorylated Tks5 targets through its

Development (2015) 142, 486-496 doi:10.1242/dev.108266

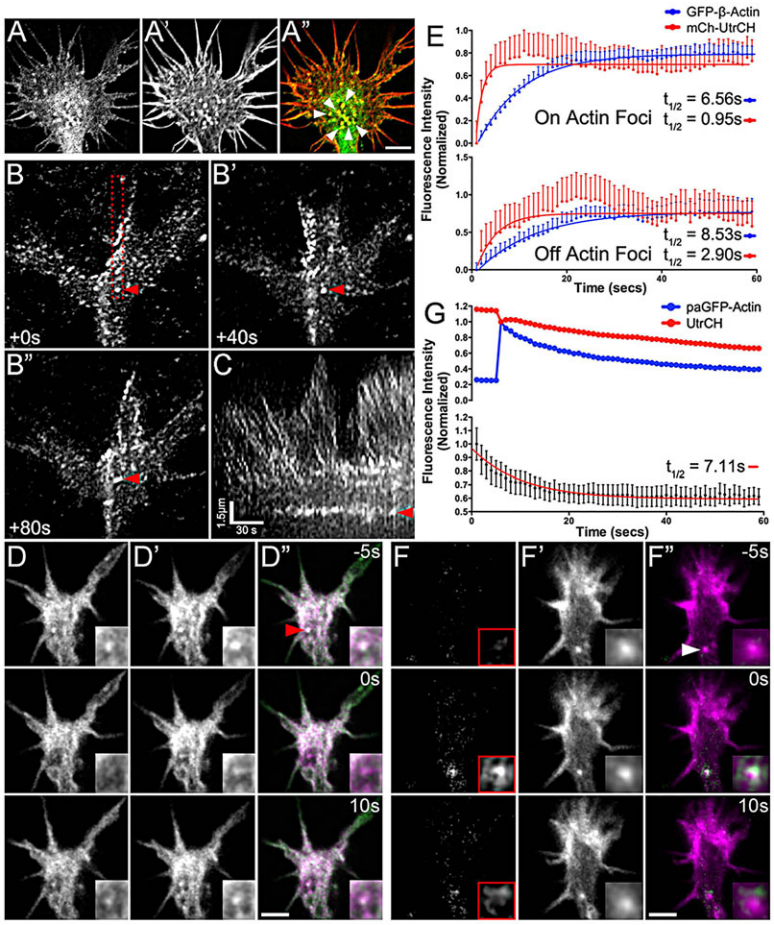

Fig. 3. F-actin foci are sites of actin polymerization. (A-A″) Confocal microscopy images of a growth cone on laminin stained for G-actin (A) and F-actin (A′). Note the colocalization of monomeric actin with F-actin foci in the merged image (A″, arrowheads). (B-B″) Time-lapse TIRF images of a live growth cone cultured on laminin and labeled with TMR-KabC. Note that stable barbed ends (arrowhead). (C) Kymograph from the boxed region in B illustrating the rearward flow of KabC-capped actin filaments (angled lines) in the P-domain and stable actin foci in the C-domain (arrowhead). (D-D″) Confocal microscopy images of a live growth cone expressing GFP-β-actin (D) together with mCh-UtrCH (D′) and an image merge (D″) during photobleaching of GFP-β-actin. Note photobleaching (0 s) and recovery (10 s) of GFP-β-actin at an mCh-UtrCH-labeled foci (arrowhead). (E) Normalized fluorescence recovery rate after photobleaching of GFP-β-actin within regions over foci (on foci, upper graph) and in regions adjacent to foci (off foci, lower graph). More rapid recovery of mCh-UtrCH is likely to be the result of a more rapid exchange rate of F-actin binding protein ($n \geq 59$). (F-F″) Confocal microscopy images of a live growth cone expressing PA-GFP-γ-actin (F) together with mCh-UtrCH (F′) and an image merge (F″) during photoactivation of PA-GFP-γ-actin. Note rapid photoactivation (0 s) and decay of PA-GFP-γ-actin at an mCh-UtrCH-labeled F-actin foci (arrowhead). (G) Normalized fluorescence decay rate after photoactivation of PA-GFP-γ-actin at foci together with slow bleaching of mCh-UtrCH signal (upper graph). The ratio of PA-GFP-γ-actin fluorescence versus that of mCh-UtrCH bleaching provides a measure of γ-actin turnover (lower graph) ($n \geq 59$). Scale bars: 5 μm (A,B,D,F); 2.5 μm (insets in D,F).

N-terminal PX domain to phosphatidylinositol containing lipid rafts (Murphy and Courtneidge, 2011). Activated Tks5 recruits additional proteins that are involved in invadosome formation, such as the actin regulators described above. To begin to understand the roles that both Tks5 and Src play in growth cone invadosomes, we examined their expression and localization. Tks5 and Tks4 were expressed in developing *Xenopus* spinal cord tissues during stages of robust axon outgrowth (Fig. 5A,B). In addition, Tks5 and active Src (phosphorylated on residue Y418, pY418-Src) localized to F-actin foci, providing strong evidence that these structures represent growth cone invadosomes (Fig. 5C; supplementary material Fig. S4). Finally, in order to visualize Tks5 dynamics in live growth cones, we expressed human Tks5, tagged with GFP (Tks5-GFP), along with mCh-UtrCH in spinal neurons. As expected, Tks5 colocalized with F-actin foci (Fig. 5E), but surprisingly these foci appeared to be more mobile compared to those foci labeled with only F-actin probes. Because Tks5 recruits several actin regulatory proteins, it is possible that overexpression of Tks5 stimulates actin polymerization, leading to mobile F-actin foci.

Both the inhibition of Src and the disruption of lipid rafts decreases invadosome number and stability in growth cones

Active Src regulates invadosome formation in non-neuronal cells through phosphorylation of both Tks5 and Cttn (Boateng and Huttenlocher, 2012). As active Src targets to growth cone invadosomes, we tested Src inhibitors on growth cone invadosome formation. As predicted, pharmacological inhibition of Src with PP2 and SU6656 resulted in fewer and less-stable invadosomes, assessed in fixed and live growth cones (Fig. 5F,G). Tks5 function is also regulated by recruitment to phosphatidylinositol 4,5-bisphosphate (PIP_2)-containing lipid rafts via its PX domain, which might be generated downstream of phosphatidylinositol (3,4,5)-trisphosphate (PIP_3) because inhibition of phosphoinositide 3-kinase (PI3K) with LY294002 blocks invadopodia formation by Src-transformed NIH-3T3 cells (Yamaguchi and Oikawa, 2010). Consistent with this, growth cones that were treated with LY294002 exhibited reduced actin foci (Fig. 5F). More generally, to test whether intact lipid rafts were necessary for growth cone invadosome formation and stability, we treated GFP-β-actin-expressing growth cones with methyl-β-cyclodextrin (MβCD). MβCD is a cholesterol-sequestering agent that has been previously shown to disrupt lipid rafts in growth cones (Guirland et al., 2004). Acute treatment of growth cones with MβCD led to a modest acceleration in the rate of neurite outgrowth and a decrease in growth cone size (Fig. 5H). Interestingly, growth cones that were treated with MβCD failed to form new stable invadosomes (Fig. 5I-J). Taken together, these results demonstrate that Src tyrosine kinases and intact lipid microdomains are required for the proper formation and maintenance of growth cone invadosomes, and provide further support for the notion that F-actin foci in growth cones are analogous to the invadosomes of invasive cells.

Invadosome protrusions extend from the C-domain of growth cones *in vitro* and *in vivo*, as revealed by 3D super-resolution microscopy

Invadosomes are often restricted to the basal surface, below the nucleus of non-neuronal cells in two-dimensional (2D) culture, whereas in 3D environments, the polymerization of actin can generate basal protrusions containing bundled F-actin (Linder et al.,

Development (2015) 142, 486-496 doi:10.1242/dev.108266

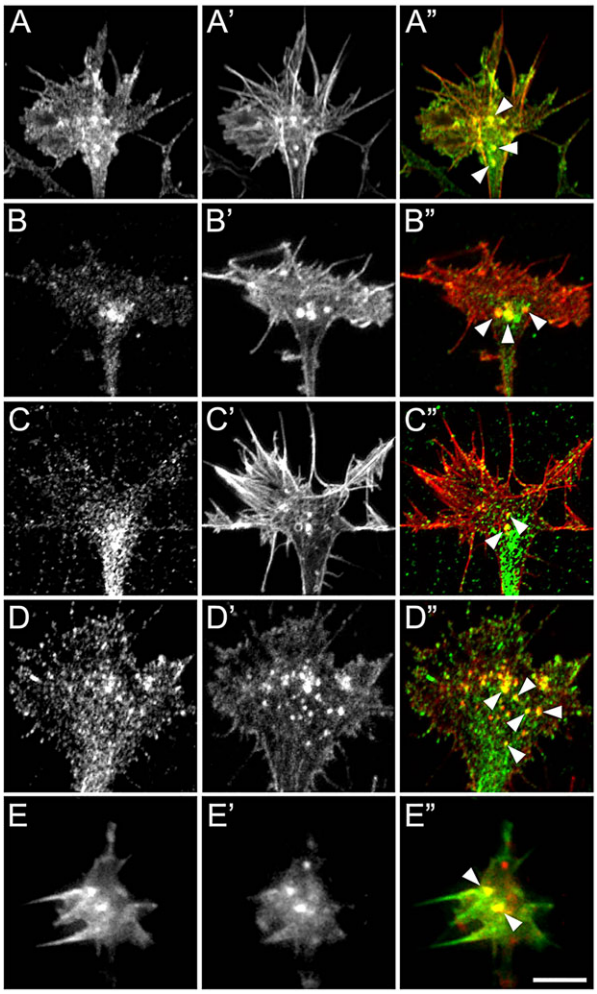

Fig. 4. F-actin foci colocalize with Cttn and other invadosome modulators within growth cones. (A-D) Confocal images of growth cones cultured on laminin and immunolabeled for Cttn (A), Arp3 (B), N-WASP (C) and Mena (D). (A′,D′) Phalloidin labeling of F-actin. (A″-D″) Merged images of the immunolabeling (green) and F-actin labeling (red). Note the strong colocalization of F-actin foci with immunolabeled proteins (arrowheads). (E-E″) TIRF images of a live growth cone on laminin expressing both GFP-α-actinin (E) and mCh-UtrCH (E′). Note in the merged image (E″) that α-actinin targets to mCh-UtrCH-labeled F-actin foci (arrowheads). Scale bar: 5 µm.

2011). To accurately resolve the cytoskeletal structure of growth cone invadosomes and to visualize their 3D projections, we used structured illumination microscopy (SIM), which can achieve a lateral resolution of 130 nm and an axial resolution of 250 nm (Toomre and Bewersdorf, 2010). Neurons cultured from embryonic *Xenopus* spinal cord, as well as iPSC-derived human forebrain neurons, were fixed and labeled for F-actin in 2D culture. Consistent with improved resolution by using SIM, we observed F-actin bundles with a fine interdigitating cross-linked actin meshwork within the peripheral veil (Fig. 6A-C). When viewed orthogonally (Fig. 6D), F-actin foci often appeared as longitudinal columns of F-actin that extended from the apical membrane of the growth cone.

Invadosomes of invasive cells often contain MTs for structural stability and for the delivery of cargo (Murphy and Courtneidge, 2011). To assess whether growth cone invadosomes contained MTs, we immunolabeled for β-tubulin together with F-actin and imaged with SIM. MTs were found alongside bundled F-actin within apical invadosomal protrusions (Fig. 6E,F). It is unclear why some invadosomes formed protrusions and contained MTs yet others remain restricted to the basal and apical surfaces of growth cones, but this is likely to depend on the 3D environment and the maturation state of the invadosome (Linder et al., 2011; Murphy and Courtneidge, 2011).

As invadosomes are stabilized by their 3D environment *in vivo*, we wanted to visualize the 3D morphology of growth cones with super resolution in collagen gel and *in vivo*. *Xenopus* explant cultures in collagen-I gels extended axons that spread in three dimensions, as detected by using low magnification confocal microscopy (supplementary material Fig. S5), and can be labeled with standard immunocytochemistry protocols for high-resolution SIM imaging. Similar to on 2D substrata, growth cones in 3D collagen that were then labeled for F-actin and Cttn exhibited punctate distributions when viewed as flattened 2D projections (Fig. 6G). However, when viewed orthogonally and as 3D rotations, F-actin and Cttn puncta often appeared as 3D protrusions that extended from the central domain of growth cones (Fig. 6H; supplementary material Movie 6). In addition, we visualized the 3D morphology of peripheral Rohon-Beard neuron growth cones in the skin by using SIM. To specifically label neurons *in vivo*, we immunolabeled whole-mount stage-25 *Xenopus* embryos using antibodies against NCAM and Cttn, and cleared the embryos with Murray's clearing solution. SIM imaging of RB neurons within the skin revealed extensive invadosome-like protrusions that extended orthogonally toward the skin from the C-domain of growth cones (Fig. 6I-K). Although growth cones *in vivo* remained largely planar with many peripheral filopodia directed along the axis of growth, discrete orthogonal protrusions could extend up to 10 µm perpendicular to the axis of extension (Fig. 6J,K; supplementary material Movie 7).

Growth cone invadosomes are sites of ECM degradation

A defining characteristic of invadosomes is their ability to degrade the local matrix, allowing cells to remodel and penetrate tissues (Linder et al., 2011). Cell surface and secreted proteases, such as the MMPs, accumulate and are released at invadosomes (Poincloux et al., 2009). To determine whether growth cone invadosomes contain MMPs, we first screened for the transcripts of known invadosomal MMP by using PCR analyses of pure spinal cord extracts. We found that MMP2, MMP9 and MMP14 were expressed in developing *Xenopus* spinal tissue (Fig. 7A), as well as several ADAM proteins (not shown). MMP14 (also known as MT1-MMP in mammals) expression in developing neurons was confirmed by immunoblotting, which revealed bands at approximately 130 kDa (not shown), 60 kDa and 30 kDa, which is likely to represent an MMP14 complex, an active form and a proteolytic fragment, respectively (Fig. 7B). To determine whether MMPs are active in the embryonic spinal cord, we performed gelatin zymography on spinal cell extracts; these showed degradation at molecular masses corresponding to the MMP9 propeptide, MMP9, the MMP2 propeptide and MMP2 (Fig. 7C). Next, to directly examine whether MMPs were present at invadosomes, we immunolabeled growth cones for MMP14 together with F-actin. Although MMP14 was present in a punctate distribution throughout growth cones, we did observe colocalization between MMP14 and F-actin foci (Fig. 7D-F). Moreover, using SIM imaging, we found that ADAM17 concentrated to the tips of invadosomal protrusions viewed in three-dimensions (Fig. 7G,H; supplementary material Movie 8).

Finally, in order to assess whether there is proteolytic activity at growth cone invadosomes, we performed fluorescent gelatin degradation assays. *Xenopus* spinal neurons were cultured on two

Development (2015) 142, 486-496 doi:10.1242/dev.108266

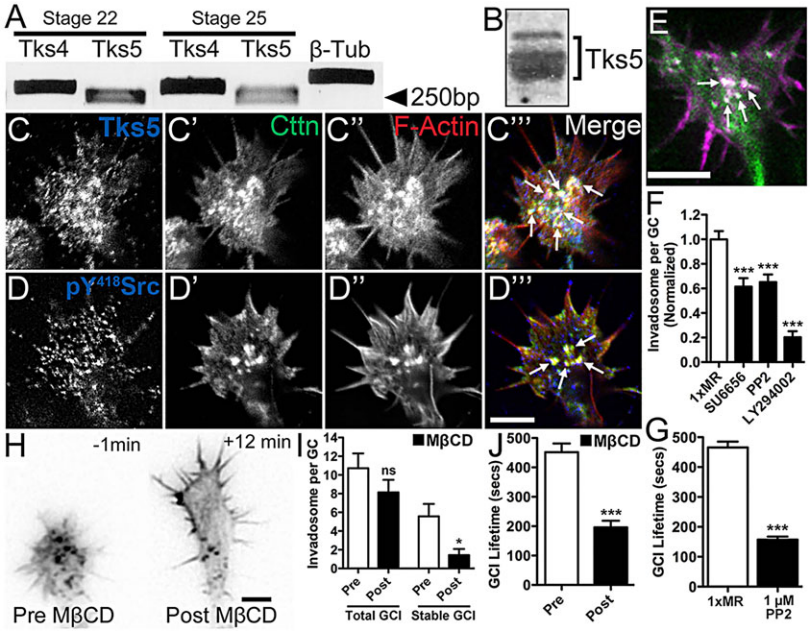

Fig. 5. F-actin foci colocalize with Src and Tks5, and require active Src and lipid rafts for their formation in growth cones. (A) Reverse transcription PCR amplification of Tks4 and Tks5 from stage-22 and stage-25 *Xenopus* spinal cord. (B) Western blot of Tks5 from stage-24 *Xenopus* spinal cord. (C,D) Confocal images of growth cones cultured on laminin and immunolabeled for Tks5 (C) and pY418-Src (D). (C′,D′) Immunolabeling of Cttn. (C″,D″) Phalloidin labeling of F-actin. (C‴-D‴) Merged images of Tks5 or Src (blue), Cttn (green) and F-actin (red). Note colocalization of Tks5 and active Src with Cttn at growth cone invadosomes (arrows). (E) TIRF image of a live growth cone on laminin expressing both Tks5-GFP (green) and mCh-UtrCH (magenta). Note that Tks5 targets to mCh-UtrCH-labeled F-actin foci (arrows). (F) Invadosome number is significantly reduced by treatment with 5 μM SU6656, 1 μM PP2 or 20 μM LY294002 for 30 min. ***P<0.0001, Kruskal–Wallis test with Dunn's post-hoc analysis, n≥75. (G) Invadosome lifetime in GFP-β-actin expressing growth cones is significantly reduced by inhibition of Src with 1 μM PP2. ***P<0.001, unpaired t-test, n≥99. (H) TIRF images of a live growth cone on laminin expressing GFP-β-actin before (left) and after (right) treatment with 2.5 μM MβCD. (I) The number of total (left) and stable (right) invadosomes in GFP-β-actin expressing growth cones is reduced after treatment with 1 μM MβCD. *P<0.05, paired t-test, n=7. (J) Invadosome lifetime in GFP-β-actin expressing growth cones is significantly reduced by cholesterol depletion with 1 μM MβCD. ***P<0.001, paired t-test, n≥57. Scale bars: 5 μm (C-E,H). ns, not significant.

variants of fluorescent gelatin that either show a loss or a gain of fluorescence upon proteolytic degradation by MMPs (Artym et al., 2009; Sloane et al., 2006). Both assays showed that growth cones exhibited a high level of proteolytic activity over regions of ECM contact, with most intense degradation occurring near F-actin foci (Fig. 7I-K; supplementary material Fig. S6). Importantly, ECM degradation was attenuated in growth cones cultured in the presence of GM6001, a non-specific MMP inhibitor, as well as in growth cones that had been treated with the invadosome disrupting agents PP2, SU6656 and MβCD (Fig. 7L). Finally, growth cones and neural crest cells expressing a dominant-negative variant of Tks5, ΔPX-Tks5 (Fig. 7L; supplementary material Fig. S7), also showed reduced ECM degradation. This specific manipulation allowed actin foci to form, but foci were highly mobile (supplementary material Movie 9), possibly due to the inability of mutant Tks5 to dock with PIP_2-containing microdomains (Abram et al., 2003; Oikawa et al., 2012; Seals et al., 2005). Taken together, these results suggest that MMPs are present and active within the developing spinal cord, and target to growth cone invadosomes where they remodel the local ECM.

Invadosomes are required for proper extension of motoneuron axons into the peripheral myotome

We hypothesize that growth cone invadosomes promote axon extension across tissue barriers, as reported previously for both normal and metastatic migratory cells (Linder et al., 2011; Murphy and Courtneidge, 2011). One location that we expect invadosomes will function is at sites where motoneurons exit the spinal cord and extend into the peripheral axial myotomal tissues. To begin to test this notion, we expressed GFP-tagged ΔPX-Tks5 or GFP by using blastomere injection at the eight-cell stage, thereby targeting dominant-negative Tks5 or control GFP to the ventral spinal cord. Embryos were allowed to develop to the neural tube stage, when the pioneering motoneuron axons are exiting the spinal cord into the periphery. Note that, although other cell types were labeled using the CMV promoter, we compared embryos that had relatively sparse labeling in order to both limit potential non-cell autonomous effects and facilitate visualization of motoneurons. Fixed and methanol-dehydrated embryos were immunolabeled for GFP plus acetylated tubulin or synaptotagmin 2 (using the Znp-1 antibody), cleared with Murray's solution and imaged intact by using confocal microscopy. Three-dimensional reconstruction of motoneuron axons on the ventral fascicle near exit points revealed that motoneuron growth cones often extended peripheral protrusions from their MT-containing central domain (Fig. 8A-C). These invadosome-like protrusions were particularly evident in wild-type motoneurons labeled with the Znp-1 antibody, which labels the most distal extent of developing axons (Fig. 8D,E). Motoneuron axon terminals exhibited numerous fine protrusions that extended laterally into the periphery (Fig. 8F; supplementary material Movie 10), some of which matured into peripheral axons (Fig. 8D). Importantly, invadosome function appeared to be necessary for proper motoneuron development, as expressing dominant-negative ΔPX-Tks5-GFP in motoneurons reduced the extension of axons into the peripheral myotomal tissue (Fig. 8G-I). Although not quantified, axon extension within the spinal cord appeared to be qualitatively normal, and dominant-negative ΔPX-Tks5-GFP did not inhibit axon extension *in vitro* (not shown), suggesting a specific effect on peripheral tissue invasion. Taken together, these data suggest that motoneuron growth cones in the

Development (2015) 142, 486-496 doi:10.1242/dev.108266

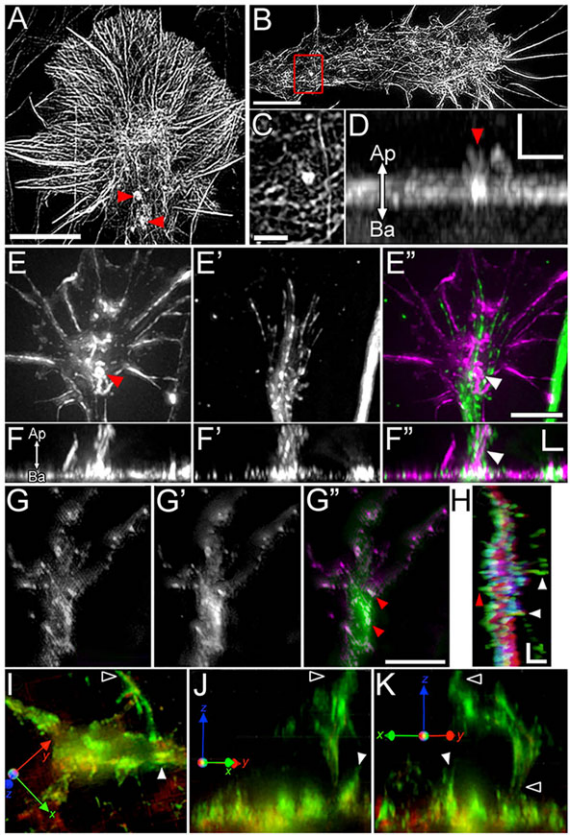

Fig. 6. F-actin-rich protrusion from the central domain of growth cones are detected by 3D SIM. (A,B) SIM images of *Xenopus* spinal neuron growth cones on laminin (A) or thin gelatin (B), fixed and stained for F-actin with Alexa-568 phalloidin. Note the cross-linked actin meshwork within the peripheral veil and the F-actin-rich foci within the growth cone central domain (arrowhead in A and red box in B). (C) 2.5× zoom of the boxed region in B. (D) Orthogonal view (*y*-*z*) through the F-actin-rich foci shown in C. Note this F-actin foci spans from the basal (Ba) substratum to the apical (Ap) membrane where it protrudes from the growth cone surface (arrowhead). (E,E′) SIM images of an iPSC-derived human forebrain neuron growth cone on laminin, fixed and stained for F-actin with Alexa-568 phalloidin (E) and immunolabeled for βIII-tubulin (E′). Note the F-actin-rich foci located within the growth cone central domain (arrowhead). (E″) Merged image of F-actin (magenta) and βIII-tubulin (green) labeling. (F-F″) Orthogonal view (*x*-*z*) images through the F-actin-rich foci shown in E-E″. Note how MTs track along F-actin within the apical protrusion (arrowhead). (G-G″) 3D SIM images of a *Xenopus* spinal neuron growth cone in a collagen-I gel stained for F-actin (G) with phalloidin and immunolabeled for Cttn (G′). Note in the merge image (G″) F-actin-rich foci (purple) within the C-domain colocalize with Cttn (green, arrowheads in G″). (H) Orthogonal view of a triple-labeled growth cone (Cttn, green; F-actin, red; βI+II tubulin, blue) in a collagen-I gel showing apical (white arrowheads) and basal protrusions (red arrowhead). (I-K) 3D SIM images of a peripheral Rohon-Beard growth cone in the skin immunolabeled for NCAM (green) and Cttn (red) and viewed at three orientations. Cttn-containing NCAM puncta in the C-domain viewed in *x*-*y* (I, solid arrowhead) associates with an apical protrusion viewed as a 90° rotation along the *x*-axis (J, solid arrowhead). A second prominent apical protrusion (open arrowheads) extends ∼10 µm toward the peripheral skin as seen in a 90° rotation along the *y*-axis (J,K). Scale bars: 5 µm (A,B,E,G,$I_{(x,y)}$,$J_{(z)}$,$K_{(z)}$); 1 µm (C,D); 2 µm (F,H).

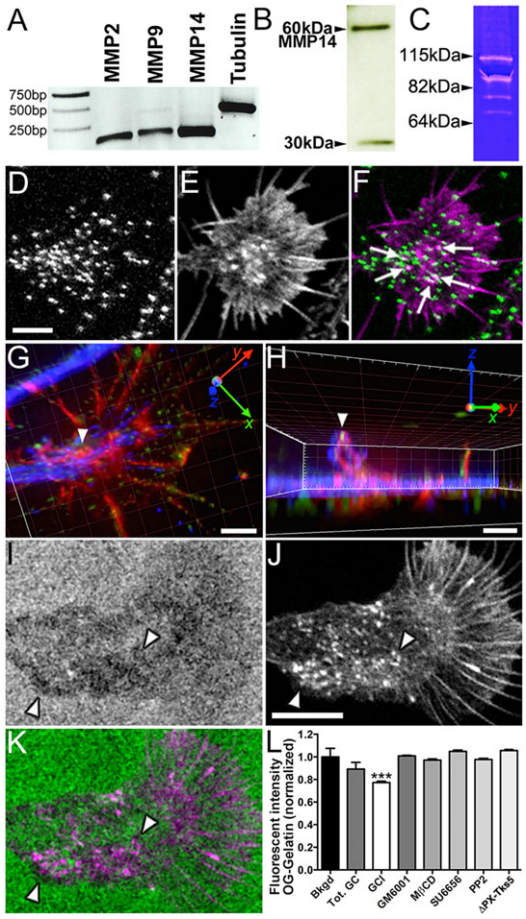

Fig. 7. Spinal neurons express MMPs, and growth cones exhibit invadosome-targeted protease activity. (A) Reverse transcription PCR amplification of *MMP2*, *MMP9* and *MMP14* from stage-24 *Xenopus* spinal cord. (B) Western blot of MMP14 from stage-24 *Xenopus* spinal cord. (C) Gelatin zymogram of MMP9 (∼90 kDa) and MMP2 (70 kDa) along with their pro-forms (∼110 kDa and ∼75 kDa, respectively) from stage-24 *Xenopus* spinal cord. (D-F) Confocal images of a spinal neuron grown on laminin and immunolabeled for MMP14 (MT1-MMP) (D), with F-actin-labeled with phalloidin (E) and an image merge (F) of MMP14 (green) and F-actin (magenta). Note colocalization of MMP14 puncta at F-actin foci (arrows). (G,H) 3D rendering view of SIM images of a human forebrain neuron growth cone (from Fig. 6E) triple-labeled for F-actin (red), βIII tubulin (blue) and ADAM17 (green). A view of the apical surface (G) shows an F-actin foci in the central domain (arrowhead), which is revealed to be an apically directed protrusion in a lateral view (H) with ADAM17 at the protrusion tip (arrowhead). (I-L) Gelatin degradation by a spinal neuron growth cone occurs near F-actin foci. (I) Oregon Green gelatin used as the substratum. (J) Growth cone labeled with Alexa-546 phalloidin. (K) Merged image of the gelatin (green) and F-actin (magenta) labels. Note colocalization of F-actin foci with areas of gelatin degradation (arrowheads). (L) Quantification of gelatin degradation for the total growth cone (Tot. GC) and at growth cone invadosomes (GCI) compared to background fluorescence. Gelatin degradation at invadosomes was inhibited by treatment with 10 µM GM6001, 2 µM PP2, 5 µM SU6656, 2.5 µM MβCD and in growth cones expressing ΔPX-Tks5-GFP. ***P<0.0001, Kruskal–Wallis test with Dunn's post-hoc analysis, n≥22. Scale bars: 5 µm (D-F); 3 µm (G,H); 10 µm (I-K).

spinal cord use invadosomes to promote axon extension into the peripheral myotome.

DISCUSSION

Many studies have identified F-actin-rich protrusions from the basal surface of invasive cells as sites of membrane attachment and degradation of the ECM, but analogous structures have not been reported in developing neuronal growth cones. In this study, we show for the first time that growth cones form 3D protrusions, which share many characteristics of invasive cell invadosomes. We found that distinct F-actin foci formed within the C-domain of growth cones from a variety of neuron types and species *in vitro*, as well as in the spinal cord and skin of intact *Xenopus* embryos. Growth cone invadosomes contained β1 integrin receptors and recruited PXN and

Development (2015) 142, 486-496 doi:10.1242/dev.108266

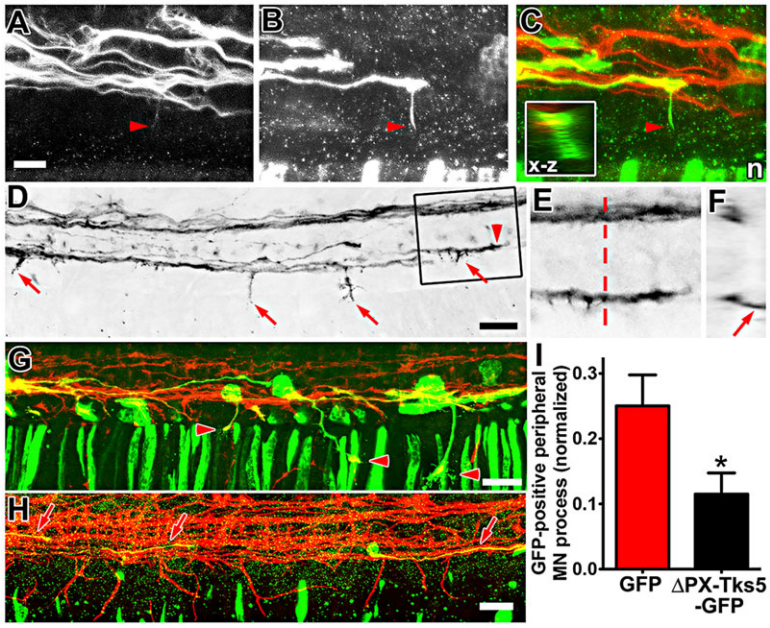

Fig. 8. Motoneuron growth cones in the spinal cord extend invadosome-like protrusions toward the peripheral myotome, which are necessary for proper axon extension into the periphery. (A,B) Maximum *z*-series projected images of a whole-mount embryo (lateral view, anterior left) with descending motoneuron growth cones on the ventral fascicle labeled with GFP by using targeted blastomere injection. This embryo was immunolabeled for βI+II tubulin (A) and GFP (B). (C) Merged image of motoneurons labeled for tubulin (red) and GFP (green) showing a robust protrusion that extends toward the notochord (n) from the central domain of the lead growth cone. Note that a MT has polymerized into this invadosome-like protrusion (A, arrowhead) that extends diagonally away from the spinal cord, as seen in an *x*-*z* view (C, inset). (D) Maximum *z*-series projected image (inverted contrast) of a whole-mount embryo (lateral view, anterior left) immunolabeled with the Znp-1 antibody. Note several peripheral axons and fine protrusions extend from motoneurons (arrows). (E) Magnified image from the boxed region in D shows a terminal motoneuron growth cone with many fine protrusions. (F) *x*-*z* view resampled along the dashed line in E shows an invadosome-like protrusion that extends deep into the lateral tissue (arrow). (G,H) Maximum *z*-series projected images of whole-mount embryos (lateral view, anterior left) expressing GFP (G) or ΔPX-Tks5-GFP (H) in motoneurons. Embryos were immunolabeled for βI+II tubulin (red) and GFP (green). Note that several peripheral GFP-expressing motoneuron axons with growth cones (G, arrowheads) have exited the spinal cord en route to the peripheral myotome, whereas motoneurons expressing ΔPX-Tks5-GFP remain within the spinal cord (H, arrows). (I) The percentage of tubulin-positive peripheral motoneuron axons that express ΔPX-Tks5-GFP is significantly less than that expressing GFP in control embryos (see Materials and Methods). **P*<0.05, Fisher's exact test. The *n* values for numbers of peripheral axons (tubulin-positive, GFP-positive), image *z* stacks and embryos, respectively, are 64, 14, 28, 7 for control and 140, 16, 32, 8 for experimental conditions. Scale bars: 10 µm (A-C); 30 µm (D,G,H).

FAK transiently, yet they were distinct from leading edge PC adhesions. Invadosomes appeared to be sites of F-actin polymerization as they contained F-actin barbed ends, as well as actin monomers, and underwent rapid actin turnover, as determined by using FRAP and FDAP. Consistent with this notion, the actin regulatory proteins Arp3, N-WASP, α-actinin and Mena localized to invadosomes. Importantly, the classic invadosome markers Cttn, pY418-Src and Tks5 robustly concentrated at growth cone invadosomes. Pharmacological manipulations suggested that Src and lipid rafts, known Tks5-targeting signals, were both necessary for invadosome formation in growth cones. Viewing growth cones by using super-resolution microscopy showed that F-actin within invadosomes oriented as axial columns, perpendicular to the direction of axon extension. Moreover, a subset of axial F-actin bundles, which often contained MTs, penetrated the apical cell surface of growth cones to form protrusions in 2D and 3D culture, as well as *in vivo*. These growth cone invadosomes targeted MMPs and locally remodeled the ECM through proteolytic activity, which required Tks5 function. Finally, dominant interference of Tks5 function *in vivo* inhibited the exit of motoneurons from the spinal cord into the periphery. Taken together, these findings demonstrate that growth cones form protrusions analogous to the invadosomes of invasive cells, which control axon guidance through 3D environments of the developing nervous system.

Invadopodia and podosomes are collectively referred to as invadosomes, although they have some notable differences in structure and function (Linder et al., 2011; Murphy and Courtneidge, 2011). Three common functions ascribed to invadosomes are cell adhesion, matrix degradation and mechanosensing (Alexander et al., 2008; Collin et al., 2008; Juin et al., 2013). Our evidence suggested that neuronal growth cones form invadosomes that share common functions to both invadopodia and podosomes (supplementary material Fig. S8). For example, growth cone invadosomes appeared to be adhesive structures, because stable F-actin foci localized to areas that were in close contact to the substratum and colocalized with adhesion-related proteins, such as integrin receptors, PXN and FAK (Fig. 2). However, although invadosomes are likely to be adhesive contacts, they differ from PCs, which typically assemble within filopodia and are short-lived (~2.5 min). Interestingly, a subset of PCs appeared to transition into invadosomes (Fig. 2E-H), and we suspect that these two processes could be linked (Chan et al., 2009; Liu et al., 2010). It is noteworthy that the F-actin foci that we observed in growth cones share many similarities to actin patches that have been found to be responsible for collateral branching of chick DRG axons (Ketschek and Gallo, 2010; Spillane et al., 2011).

Two important questions are what extracellular cues and intracellular signals instruct invadosome formation versus PC formation in growth cones? In non-neuronal cells, the formation of invadosomes is stimulated by growth factors, such as platelet-derived growth factor (PDGF), transforming growth factor-β (TGFβ) and epidermal growth factor (EGF) (Murphy and Courtneidge, 2011). These growth factors activate Src tyrosine

Development (2015) 142, 486-496 doi:10.1242/dev.108266

kinases, which phosphorylate Tks5, Cttn and other key regulatory proteins that target to invadosomes. Consistent with a role for Src in growth cone invadosomes, we found that active Src targeted to invadosomes and that inhibition of Src reduced invadosome formation (Fig. 5F,G). Other intracellular signaling proteins, such as protein kinase C (PKC) and PI3K cooperate with Src in regulating invadosome formation (Hoshino et al., 2012; Yamaguchi et al., 2011). PI3K might initiate the formation of invadosomes through local production of PIP_3 and PIP_2, which recruits Tks5 through association with its N-terminal PX domain (Hoshino et al., 2013; Yamaguchi and Oikawa, 2010). Consistent with a similar role in growth cones, we found that pharmacological inhibition of PI3K, as well as expression of ΔPX-Tks5-GFP, reduced and mobilized F-actin foci, respectively, and limited ECM degradation (Fig. 5G, Fig. 7L; supplementary material Movie 9). Because several growth factors and axon guidance cues, such as brain-derived growth factor (BDNF), netrin and ephrins are known to regulate Src, PKC and PI3K function in growth cones (Dent et al., 2011; Hall and Lalli, 2010), we hypothesize that guidance cues in combination with specific ECM proteins control PC-mediated substratum adhesion versus invadosome-mediated basal lamina penetration.

Another crucial open question is what roles do invadosomes have in the guidance of axons and dendrites to their synaptic targets? One possible function of invadosomes is the targeting of MMPs and other proteases, such as ADAMs, in order to promote local matrix degradation and the extension of axons through tissues (McFarlane, 2003; Yong et al., 2001), and we found that these MMPs target to growth cone invadosomes (Fig. 7). Neural crest cells form invadosomes that are necessary for their proper migration, the development of craniofacial structures and pigmentation in zebrafish embryos (Murphy et al., 2011). Matrix proteases might regulate axon extension in part by degrading the surrounding matrix to create a passage for axonal outgrowth (Gutierrez-Fernandez et al., 2009; Hayashita-Kinoh et al., 2001; Zuo et al., 1998), but more recent studies that were performed both *in vitro* and *in vivo* now suggest that proteolytic cleavage is directed toward specific ligands in the environment, as well as towards receptors on growth cones in order to activate or terminate motility (Chen et al., 2007; Fambrough et al., 1996; Hehr et al., 2005; Schimmelpfeng et al., 2001; Webber et al., 2002). For example, MMPs are necessary for the conversion of pro-neurotrophins into mature neurotrophins (Lee et al., 2001) and during ectodomain shedding of guidance cue receptors (Bai et al., 2011; Browne et al., 2012; Coleman et al., 2010; Galko and Tessier-Lavigne, 2000; Hattori et al., 2000; Kanning et al., 2003; Lin et al., 2008; Miller et al., 2008; Walmsley et al., 2004). We found that commissural interneurons near the midline formed robust F-actin foci (Fig. 1G) that could be invadosomes interacting with cues within the ventral floorplate. Also, we showed that invadosomes are necessary for motoneuron axon exit from the spinal cord into the peripheral myotome (Fig. 8). However, a specific role for MMPs has not been established at these choice points, nor has the morphogen that promotes invadosome formation by these growth cones been identified. Future studies will examine candidate morphogens, such as BDNF or pro-BDNF, that might be released by myocytes (Yang et al., 2009) to regulate peripheral sprouting of invadosomes.

MATERIALS AND METHODS

Reverse-transcription PCR and primers

Primers against *Tks5*, *MMP2*, *MMP9* and *MMP14* were designed from *Xenopus laevis* sequences (Xenbase; Bowes et al., 2010) using Primer3 (Rozen and Skaletsky, 2000), and were then synthesized at the Biotechnology Center (University of Wisconsin, Madison). *Tks5* and *MMP* transcripts were amplified by using PCR from reverse transcribed mRNA isolated with TRIzol (Invitrogen) from spinal cord tissues of stage-24 to stage-26 embryos.

Embryo injection and cell culture

Xenopus laevis embryos were obtained and staged as described previously (Gomez et al., 2003). For protein expression experiments, eight-cell stage embryos were injected with 0.25 ng of *in vitro*-transcribed capped mRNA (mMessage Machine, Ambion) or 60-70 pg of DNA (constructs are detailed in the methods in the supplementary material). Neural tube and retinal cultures were prepared as described previously (Gomez et al., 2003; Woo and Gomez, 2006). For 3D cultures, explants were cultured onto 1.5 mg/ml collagen-I gels (BD Biosciences). Cultures were imaged or fixed 18-22 h after plating. All methods were approved by the University of Wisconsin School of Public Heath Animal Care and Use Committee.

Human neurons derived from iPSCs

Human neurons were differentiated from iPSCs as previously described (Gamm et al., 2008; Hu and Zhang, 2009; Liu et al., 2013; Pankratz et al., 2007). Neurospheres were plated onto glass coverslips coated with poly-D-lysine (PDL) and laminin (PDL-LN) and cultured in neural basal media with B27 supplements (Gibco).

Fluorescent gelatin degradation assay

Fluorescent gelatin-coated coverslips were prepared as described previously (Artym et al., 2009). Briefly, coverslips were coated with 50 µg/ml PDL and activated with 0.5% glutaraldehyde, followed by conjugation with Oregon Green 488 gelatin (Invitrogen) or Cy3 gelatin (Millipore) for 10 min at room temperature. Residual reactive groups were quenched with sodium borohydride. The matrix protease inhibitor GM6001 (10 µM) was applied overnight, whereas PP2, SU6656 and MβCD were applied for 4 h before fixation. Coverslips coated with DQ collagen-IV (Invitrogen) were prepared as described previously (Sloane et al., 2006). Briefly, coverslips were coated with a solution containing 25 µg/ml laminin, fibronectin and DQ collagen-IV. Cultures were fixed 18-22 h after plating and imaged by using confocal microscopy. Further details of the reagents and microscopy analysis used can be found in the methods in the supplementary material.

Immunoblotting and immunocytochemistry

Tks5 and MMP14 were blotted from total protein extracts from stage-24 to stage-26 embryo spinal cords using the Novex NuPAGE SDS-PAGE gel system (Invitrogen). Tks5 (1:500) and MMP14 (1:1000) primary antibodies and horseradish peroxidase (HRP)-conjugated secondary antibodies (1:5000, Jackson ImmunoResearch) were used, and the blots were developed by using enhanced chemiluminescence (ThermoScientific Pierce ECL).

Neurons in 2D culture were immunolabeled as described previously (Myers and Gomez, 2011; Santiago-Medina et al., 2013). Three-dimensional cultures were fixed for 1 h and blocked in Ca^{2+}- Mg^{2+}-free (CMF)-PBS containing 0.5% fish gelatin and 0.2% Triton X-100 (GBT, gelatin block with Triton) overnight at 4°C. See methods in the supplementary material for antibody details.

Gelatin zymography

Gelatin zymography was performed using stage-24 to stage-26 *Xenopus* embryo spinal cords. Lysates were run on a Novex zymogram gelatin gel and processed according to the manufacturer's instructions (Invitrogen).

Whole-mount embryo dissection and imaging

To detect F-actin in motoneurons and commissural interneurons *in vivo*, mCh-UtrCH or GFP-UtrCH was expressed by using targeted blastomere injection of mRNA. For imaging of commissural interneurons, embryos were fixed at stage 23 to stage 25 and dissected to expose the spinal cord as described previously (Moon and Gomez, 2005). Peripheral Rohon-Beard and motoneuron growth cones were imaged within intact stage-24 to stage-25 embryos that were fixed in 4% PFA in sucrose, dehydrated in methanol and cleared, as described previously (Huang et al., 2007). Undissected embryos were immunolabeled in GBT solution for NCAM (HNK-1

antibody) and Cttn for Rohon-Beard neurons, or GFP, Znp-1 and acetylated tubulin for motoneurons. After immunolabeling and dehydration, embryos were cleared in Murray's solution (2:1 benzyl benzoate:benzyl alcohol) and imaged by using 3D confocal microscopy. Further details of the 3D microscopy are given in the methods in the supplementary material. To quantify the percentage of peripheral motoneuron process extensions, we counted the total number of tubulin-positive peripheral axons and the total number of GFP-positive (GFP or ΔPX-Tks5-GFP) peripheral axons (double labeled). The percentage of tubulin-positive peripheral axons that were also GFP-positive was calculated for each *z*-stack to determine variability and significance between groups. The extent of motoneuron labeling was qualitatively similar between experiment and control embryos.

Acknowledgements
We thank Erik Dent and members of the Gomez lab for comments on the manuscript; Tom Fothergill, Derrick McVicker and Diana Cowdrey for providing mouse embryonic hippocampal and cortical cultures; and Zhen Huang, Shang Ma and Hyo Jun Kwon for the gelatin zymography.

Competing interests
The authors declare no competing or financial interests.

Author contributions
M.S.-M. and T.M.G. designed the study; M.S.-M., K.A.G. and T.M.G. performed the research and analyzed the data; R.H.N. and S.M.O. provided some *in vivo* images and human neuronal cultures; M.S.-M. and T.M.G. wrote the paper.

Funding
This work was supported by the National Institutes of Health [NS41564 and NS088477 to T.M.G.] and by a diversity supplement to M.S.-M. Deposited in PMC for release after 12 months.

Supplementary material
Supplementary material available online at
http://dev.biologists.org/lookup/suppl/doi:10.1242/dev.108266/-/DC1

References
Abram, C. L., Seals, D. F., Pass, I., Salinsky, D., Maurer, L., Roth, T. M. and Courtneidge, S. A. (2003). The adaptor protein fish associates with members of the ADAMs family and localizes to podosomes of Src-transformed cells. *J. Biol. Chem.* **278**, 16844-16851.

Alexander, N. R., Branch, K. M., Parekh, A., Clark, E. S., Iwueke, I. C., Guelcher, S. A. and Weaver, A. M. (2008). Extracellular matrix rigidity promotes invadopodia activity. *Curr. Biol.* **18**, 1295-1299.

Artym, V. V., Yamada, K. M. and Mueller, S. C. (2009). ECM degradation assays for analyzing local cell invasion. *Methods Mol. Biol.* **522**, 211-219.

Bai, G., Chivatakarn, O., Bonanomi, D., Lettieri, K., Franco, L., Xia, C., Stein, E., Ma, L., Lewcock, J. W. and Pfaff, S. L. (2011). Presenilin-dependent receptor processing is required for axon guidance. *Cell* **144**, 106-118.

Boateng, L. R. and Huttenlocher, A. (2012). Spatiotemporal regulation of Src and its substrates at invadosomes. *Eur. J. Cell Biol.* **91**, 878-888.

Bowes, J. B., Snyder, K. A., Segerdell, E., Jarabek, C. J., Azam, K., Zorn, A. M. and Vize, P. D. (2010). Xenbase: gene expression and improved integration. *Nucleic Acids Res.* **38** Suppl. 1, D607-D612.

Browne, K., Wang, W., Liu, R. Q., Piva, M. and O'Connor, T. P. (2012). Transmembrane semaphorin5B is proteolytically processed into a repulsive neural guidance cue. *J. Neurochem.* **123**, 135-146.

Chan, K. T., Cortesio, C. L. and Huttenlocher, A. (2009). FAK alters invadopodia and focal adhesion composition and dynamics to regulate breast cancer invasion. *J. Cell Biol.* **185**, 357-370.

Chen, Y., Hehr, C. L., Atkinson-Leadbeater, K., Hocking, J. C. and McFarlane, S. (2007). Targeting of retinal axons requires the metalloproteinase ADAM10. *J. Neurosci.* **27**, 8448-8456.

Coleman, H. A., Labrador, J.-P., Chance, R. K. and Bashaw, G. J. (2010). The Adam family metalloprotease Kuzbanian regulates the cleavage of the roundabout receptor to control axon repulsion at the midline. *Development* **137**, 2417-2426.

Collin, O., Na, S., Chowdhury, F., Hong, M., Shin, M. E., Wang, F. and Wang, N. (2008). Self-organized podosomes are dynamic mechanosensors. *Curr. Biol.* **18**, 1288-1294.

Courtneidge, S. A. (2012). Cell migration and invasion in human disease: the Tks adaptor proteins. *Biochem. Soc. Trans.* **40**, 129-132.

Decourt, B., Munnamalai, V., Lee, A. C., Sanchez, L. and Suter, D. M. (2009). Cortactin colocalizes with filopodial actin and accumulates at IgCAM adhesion sites in Aplysia growth cones. *J. Neurosci. Res.* **87**, 1057-1068.

Dent, E. W., Gupton, S. L. and Gertler, F. B. (2011). The growth cone cytoskeleton in axon outgrowth and guidance. *Cold Spring Harb. Perspect. Biol.* **3**, a001800.

Fambrough, D., Pan, D., Rubin, G. M. and Goodman, C. S. (1996). The cell surface metalloprotease/disintegrin Kuzbanian is required for axonal extension in Drosophila. *Proc. Natl. Acad. Sci. USA* **93**, 13233-13238.

Galko, M. J. and Tessier-Lavigne, M. (2000). Function of an axonal chemoattractant modulated by metalloprotease activity. *Science* **289**, 1365-1367.

Gamm, D. M., Melvan, J. N., Shearer, R. L., Pinilla, I., Sabat, G., Svendsen, C. N. and Wright, L. S. (2008). A novel serum-free method for culturing human prenatal retinal pigment epithelial cells. *Invest. Ophthalmol. Vis. Sci.* **49**, 788-799.

Gomez, T. M., Roche, F. K. and Letourneau, P. C. (1996). Chick sensory neuronal growth cones distinguish fibronectin from laminin by making substratum contacts that resemble focal contacts. *J. Neurobiol.* **29**, 18-34.

Gómez, T. M., Harrigan, D., Henley, J. and Robles, E. (2003). Working with Xenopus spinal neurons in live cell culture. *Methods Cell Biol.* **71**, 129-156.

Guirland, C., Suzuki, S., Kojima, M., Lu, B. and Zheng, J. Q. (2004). Lipid rafts mediate chemotropic guidance of nerve growth cones. *Neuron* **42**, 51-62.

Gutierrez-Fernandez, A., Gingles, N. A., Bai, H., Castellino, F. J., Parmer, R. J. and Miles, L. A. (2009). Plasminogen enhances neuritogenesis on laminin-1. *J. Neurosci.* **29**, 12393-12400.

Hall, A. and Lalli, G. (2010). Rho and Ras GTPases in axon growth, guidance, and branching. *Cold Spring Harb. Perspect. Biol.* **2**, a001818.

Hattori, M., Osterfield, M. and Flanagan, J. G. (2000). Regulated cleavage of a contact-mediated axon repellent. *Science* **289**, 1360-1365.

Hayashita-Kinoh, H., Kinoh, H., Okada, A., Komori, K., Itoh, Y., Chiba, T., Kajita, M., Yana, I. and Seiki, M. (2001). Membrane-type 5 matrix metalloproteinase is expressed in differentiated neurons and regulates axonal growth. *Cell Growth Differ.* **12**, 573-580.

Hehr, C. L., Hocking, J. C. and McFarlane, S. (2005). Matrix metalloproteinases are required for retinal ganglion cell axon guidance at select decision points. *Development* **132**, 3371-3379.

Hoshino, D., Jourquin, J., Emmons, S. W., Miller, T., Goldgof, M., Costello, K., Tyson, D. R., Brown, B., Lu, Y., Prasad, N. K. et al. (2012). Network analysis of the focal adhesion to invadopodia transition identifies a PI3K-PKCalpha invasive signaling axis. *Sci. Signal.* **5**, ra66.

Hoshino, D., Branch, K. M. and Weaver, A. M. (2013). Signaling inputs to invadopodia and podosomes. *J. Cell Sci.* **126**, 2979-2989.

Hu, B.-Y. and Zhang, S.-C. (2009). Differentiation of spinal motor neurons from pluripotent human stem cells. *Nat. Protoc.* **4**, 1295-1304.

Huang, J. K., Dorey, K., Ishibashi, S. and Amaya, E. (2007). BDNF promotes target innervation of Xenopus mandibular trigeminal axons in vivo. *BMC Dev. Biol.* **7**, 59.

Juin, A., Planus, E., Guillemot, F., Horakova, P., Albiges-Rizo, C., Génot, E., Rosenbaum, J., Moreau, V. and Saltel, F. (2013). Extracellular matrix rigidity controls podosome induction in microvascular endothelial cells. *Biol. Cell* **105**, 46-57.

Kanning, K. C., Hudson, M., Amieux, P. S., Wiley, J. C., Bothwell, M. and Schecterson, L. C. (2003). Proteolytic processing of the p75 neurotrophin receptor and two homologs generates C-terminal fragments with signaling capability. *J. Neurosci.* **23**, 5425-5436.

Keren, K., Pincus, Z., Allen, G. M., Barnhart, E. L., Marriott, G., Mogilner, A. and Theriot, J. A. (2008). Mechanism of shape determination in motile cells. *Nature* **453**, 475-480.

Ketschek, A. and Gallo, G. (2010). Nerve growth factor induces axonal filopodia through localized microdomains of phosphoinositide 3-kinase activity that drive the formation of cytoskeletal precursors to filopodia. *J. Neurosci.* **30**, 12185-12197.

Kirkbride, K. C., Sung, B. H., Sinha, S. and Weaver, A. M. (2011). Cortactin: a multifunctional regulator of cellular invasiveness. *Cell Adh. Migr.* **5**, 187-198.

Kolodkin, A. L. and Tessier-Lavigne, M. (2011). Mechanisms and molecules of neuronal wiring: a primer. *Cold Spring Harb. Perspect. Biol.* **3**, a001727.

Kurklinsky, S., Chen, J. and McNiven, M. A. (2011). Growth cone morphology and spreading are regulated by a dynamin-cortactin complex at point contacts in hippocampal neurons. *J. Neurochem.* **117**, 48-60.

Lee, R., Kermani, P., Teng, K. K. and Hempstead, B. L. (2001). Regulation of cell survival by secreted proneurotrophins. *Science* **294**, 1945-1948.

Lee, C. W., Vitriol, E. A., Shim, S., Wise, A. L., Velayutham, R. P. and Zheng, J. Q. (2013). Dynamic localization of G-actin during membrane protrusion in neuronal motility. *Curr. Biol.* **23**, 1046-1056.

Lin, K.-T., Sloniowski, S., Ethell, D. W. and Ethell, I. M. (2008). Ephrin-B2-induced cleavage of EphB2 receptor is mediated by matrix metalloproteinases to trigger cell repulsion. *J. Biol. Chem.* **283**, 28969-28979.

Linder, S., Wiesner, C. and Himmel, M. (2011). Degrading devices: invadosomes in proteolytic cell invasion. *Annu. Rev. Cell Dev. Biol.* **27**, 185-211.

Liu, S., Yamashita, H., Weidow, B., Weaver, A. M. and Quaranta, V. (2010). Laminin-332-beta1 integrin interactions negatively regulate invadopodia. *J. Cell. Physiol.* **223**, 134-142.

Liu, Y., Weick, J. P., Liu, H., Krencik, R., Zhang, X., Ma, L., Zhou, G.-m., Ayala, M. and Zhang, S.-C. (2013). Medial ganglionic eminence-like cells derived from

human embryonic stem cells correct learning and memory deficits. *Nat. Biotechnol.* **31**, 440-447.
Lowery, L. A. and Van Vactor, D. (2009). The trip of the tip: understanding the growth cone machinery. *Nat. Rev. Mol. Cell Biol.* **10**, 332-343.
MacGrath, S. M. and Koleske, A. J. (2012). Cortactin in cell migration and cancer at a glance. *J. Cell Sci.* **125**, 1621-1626.
Marsick, B. M., Flynn, K. C., Santiago-Medina, M., Bamburg, J. R. and Letourneau, P. C. (2010). Activation of ADF/cofilin mediates attractive growth cone turning toward nerve growth factor and netrin-1. *Dev. Neurobiol.* **70**, 565-588.
McFarlane, S. (2003). Metalloproteases: carving out a role in axon guidance. *Neuron* **37**, 559-562.
Medeiros, N. A., Burnette, D. T. and Forscher, P. (2006). Myosin II functions in actin-bundle turnover in neuronal growth cones. *Nat. Cell Biol.* **8**, 216-226.
Miller, C. M., Page-McCaw, A. and Broihier, H. T. (2008). Matrix metalloproteinases promote motor axon fasciculation in the Drosophila embryo. *Development* **135**, 95-109.
Moon, M. S. and Gomez, T. M. (2005). Adjacent pioneer commissural interneuron growth cones switch from contact avoidance to axon fasciculation after midline crossing. *Dev. Biol.* **288**, 474-486.
Murphy, D. A. and Courtneidge, S. A. (2011). The 'ins' and 'outs' of podosomes and invadopodia: characteristics, formation and function. *Nat. Rev. Mol. Cell Biol.* **12**, 413-426.
Murphy, D. A., Diaz, B., Bromann, P. A., Tsai, J. H., Kawakami, Y., Maurer, J., Stewart, R. A., Izpisúa-Belmonte, J. C. and Courtneidge, S. A. (2011). A Src-Tks5 pathway is required for neural crest cell migration during embryonic development. *PLoS ONE* **6**, pe22499.
Myers, J. P. and Gomez, T. M. (2011). Focal adhesion kinase promotes integrin adhesion dynamics necessary for chemotropic turning of nerve growth cones. *J. Neurosci.* **31**, 13585-13595.
Oikawa, T., Oyama, M., Kozuka-Hata, H., Uehara, S., Udagawa, N., Saya, H. and Matsuo, K. (2012). Tks5-dependent formation of circumferential podosomes/invadopodia mediates cell-cell fusion. *J. Cell Biol.* **197**, 553-568.
Pankratz, M. T., Li, X.-J., LaVaute, T. M., Lyons, E. A., Chen, X. and Zhang, S.-C. (2007). Directed neural differentiation of human embryonic stem cells via an obligated primitive anterior stage. *Stem Cells* **25**, 1511-1520.
Petchprayoon, C., Suwanborirux, K., Tanaka, J., Yan, Y., Sakata, T. and Marriott, G. (2005). Fluorescent kabiramides: new probes to quantify actin in vitro and in vivo. *Bioconjug. Chem.* **16**, 1382-1389.
Philippar, U., Roussos, E. T., Oser, M., Yamaguchi, H., Kim, H.-D., Giampieri, S., Wang, Y., Goswami, S., Wyckoff, J. B., Lauffenburger, D. A. et al. (2008). A Mena invasion isoform potentiates EGF-induced carcinoma cell invasion and metastasis. *Dev. Cell* **15**, 813-828.
Poincloux, R., Lizarraga, F. and Chavrier, P. (2009). Matrix invasion by tumour cells: a focus on MT1-MMP trafficking to invadopodia. *J. Cell Sci.* **122**, 3015-3024.
Renaudin, A., Lehmann, M., Girault, J.-A. and McKerracher, L. (1999). Organization of point contacts in neuronal growth cones. *J. Neurosci. Res.* **55**, 458-471.
Robles, E. and Gomez, T. M. (2006). Focal adhesion kinase signaling at sites of integrin-mediated adhesion controls axon pathfinding. *Nat. Neurosci.* **9**, 1274-1283.
Rozen, S. and Skaletsky, H. (2000). Primer3 on the WWW for general users and for biologist programmers. *Methods Mol. Biol.* **132**, 365-386.
Santiago-Medina, M., Myers, J. P. and Gomez, T. M. (2011). Imaging adhesion and signaling dynamics in Xenopus laevis growth cones. *Dev. Neurobiol.* **72**, 585-599.
Santiago-Medina, M., Gregus, K. A. and Gomez, T. M. (2013). PAK-PIX interactions regulate adhesion dynamics and membrane protrusion to control neurite outgrowth. *J. Cell Sci.* **126**, 1122-1133.
Schimmelpfeng, K., Gögel, S. and Klämbt, C. (2001). The function of leak and kuzbanian during growth cone and cell migration. *Mech. Dev.* **106**, 25-36.
Seals, D. F., Azucena, E. F., Jr, Pass, I., Tesfay, L., Gordon, R., Woodrow, M., Resau, J. H. and Courtneidge, S. A. (2005). The adaptor protein Tks5/Fish is required for podosome formation and function, and for the protease-driven invasion of cancer cells. *Cancer Cell* **7**, 155-165.
Sloane, B. F., Sameni, M., Podgorski, I., Cavallo-Medved, D. and Moin, K. (2006). Functional imaging of tumor proteolysis. *Annu. Rev. Pharmacol. Toxicol.* **46**, 301-315.
Spillane, M., Ketschek, A., Jones, S. L., Korobova, F., Marsick, B., Lanier, L., Svitkina, T. and Gallo, G. (2011). The actin nucleating Arp2/3 complex contributes to the formation of axonal filopodia and branches through the regulation of actin patch precursors to filopodia. *Dev. Neurobiol.* **71**, 747-758.
Tanaka, J., Yan, Y., Choi, J., Bai, J., Klenchin, V. A., Rayment, I. and Marriott, G. (2003). Biomolecular mimicry in the actin cytoskeleton: mechanisms underlying the cytotoxicity of kabiramide C and related macrolides. *Proc. Natl. Acad. Sci. USA* **100**, 13851-13856.
Toomre, D. and Bewersdorf, J. (2010). A new wave of cellular imaging. *Annu. Rev. Cell Dev. Biol.* **26**, 285-314.
Walmsley, A. R., McCombie, G., Neumann, U., Marcellin, D., Hillenbrand, R., Mir, A. K. and Frentzel, S. (2004). Zinc metalloproteinase-mediated cleavage of the human Nogo-66 receptor. *J. Cell Sci.* **117**, 4591-4602.
Webber, C. A., Hocking, J. C., Yong, V. W., Stange, C. L. and McFarlane, S. (2002). Metalloproteases and guidance of retinal axons in the developing visual system. *J. Neurosci.* **22**, 8091-8100.
Woo, S. and Gomez, T. M. (2006). Rac1 and RhoA promote neurite outgrowth through formation and stabilization of growth cone point contacts. *J. Neurosci.* **26**, 1418-1428.
Yamaguchi, H. and Oikawa, T. (2010). Membrane lipids in invadopodia and podosomes: key structures for cancer invasion and metastasis. *Oncotarget* **1**, 320-328.
Yamaguchi, H., Yoshida, S., Muroi, E., Yoshida, N., Kawamura, M., Kouchi, Z., Nakamura, Y., Sakai, R. and Fukami, K. (2011). Phosphoinositide 3-kinase signaling pathway mediated by p110alpha regulates invadopodia formation. *J. Cell Biol.* **193**, 1275-1288.
Yang, F., Je, H.-S., Ji, Y., Nagappan, G., Hempstead, B. and Lu, B. (2009). Pro-BDNF-induced synaptic depression and retraction at developing neuromuscular synapses. *J. Cell Biol.* **185**, 727-741.
Yong, V. W., Power, C., Forsyth, P. and Edwards, D. R. (2001). Metalloproteinases in biology and pathology of the nervous system. *Nat. Rev. Neurosci.* **2**, 502-511.
Zuo, J., Ferguson, T. A., Hernandez, Y. J., Stetler-Stevenson, W. G. and Muir, D. (1998). Neuronal matrix metalloproteinase-2 degrades and inactivates a neurite-inhibiting chondroitin sulfate proteoglycan. *J. Neurosci.* **18**, 5203-5211.

Supplementary materials and methods

Plasmid Constructs. GFP-γ-actin (rat) was provided by Andrew Matus (Friedrich Miescher Institute, Basel, Switzerland). GFP-β-actin (human) and PA-GFP-γ-actin constructs were provided by James Zheng (Emory University, Atlanta, GA). GFP-Utrophin-CH (F-actin probe) and GFP-cortactin (*Xenopus*) were provided by William Bement (University of Wisconsin, Madison). mCherry-Rab5A and DsRed-Clathrin light chain were provided by Jon Audhya (University of Wisconsin, Madison). Paxillin–GFP (chicken) was provided by A. F. Horwitz (University of Virginia, Charlottesville, VA). GFP-α-actinin-1 (human) was provided by Carol Otey (University of North Carolina, Chapel Hill, NC). Human wild-type Tks5 and dominant negative ΔPX-Tks5 tagged with GFP were provided by Sara Courtneidge (Sanford-Burnham Medical Research Institute, La Jolla, CA).

Reagents. SU6656, PP2 and GM6001 were obtained from Calbiochem (La Jolla, CA). MβCD was purchased from Sigma. To visualize F-actin retrograde flow, cultures were loaded with 3 nM kabiramide C conjugated to TMR (TMR-KabC; provided by Gerard Marriott, University of California, Berkeley). Antibodies were used as follows: β1-integrin (8C8), SV2, Znp-1 (Synaptotagmin-2) (Developmental Studies Hybridoma Bank (DSHB)); pY118-Paxillin (44660G), pY397-FAK (44624G), pY418-Src (44660G) (Invitrogen); Cortactin (4F11), MMP14 (AB6005, Millipore); Tks5 (M-300; Santa Cruz Biotechnology), βI,II-Tubulin (T8535) and acetylated-Tubulin (T6793), HNK-1 (C0678, NCAM, Sigma); GFP (Ab6556, AbCAM). Arp3, N-

WASP and Mena were provided by Erik Dent (University of Wisconsin, Madison). Alexa Fluor 488 deoxyribonuclease I (DNase I; Invitrogen) was used to label monomeric G-actin.

Immunocytochemistry. Primary antibodies were diluted in block as follows: 1:250 β-Integrin (8C8), 1:500 pY118-Paxillin, 1:500 pY397-FAK, 1:100 SV2, 1:500 Cortactin, 1:250 Arp3, 1:250 N-WASP, 1:500 Mena, 1:500 pY418-Src, 1:250 Tks5, 1:500 βI,II-Tubulin, 1:1000 acetylated-Tubulin, 1:500 HNK-1 and 1:500 MMP14. Alexa-Fluor-conjugated secondary antibodies (Invitrogen) were used at 1:250 in blocking solution. Alexa-546 phalloidin and Alexa-647 carboxylic acid, succinimidyl ester were used at 1:100 and 1:1000 respectively.

Confocal and TIRF image acquisition and analysis. For both live and fixed fluorescence microscopy *in vitro*, images were acquired using either 60x/1.45NA objective on an Olympus Fluoview 500 laser-scanning confocal system or a 100x/1.49NA objective lens on a Nikon total internal reflection fluorescence (TIRF) microscope. FRAP and FDAP experiments were performed on a Nikon A1 confocal using a 100x/1.45NA objective. On the Olympus confocal, samples were imaged at 2.5x zoom (pixel size = 165 nm). Live explant cultures were sealed within perfusion chambers as described (Gomez et al., 2003) to allow rapid exchange of solutions. Whole mount Z stacks (1-2 um step size) were captured using a 60x/1.1 NA water objective. Images were analyzed using ImageJ software (W. Rasband, National

Institutes of Health, Bethesda, MD) and volumes were rendered using Volocity software.

Structured illumination microscopy image acquisition. High-resolution structured illumination (SIM) Z-stacks were captured using a DeltaVision OMX microscope (Applied Precision), an ELYRA PS.1 microscope (Carl Zeiss Microscopy) or a N-SIM microscope (Nikon). The DeltaVision OMX V4 3D SIM platform with Blaze technology was used with a 60x/1.42 Plan-Apo N objective (Olympus), excitation wavelengths of 488, 561 and 635 nm and 3 sCMOS cameras. Images were acquired using DeltaVision software and deconvolved using softWoRx image processing software (Applied Precision). The ELYRA was used with either a 63x/1.4 Plan-Apochromat or 100x/1.46 α-Plan-Apochromat objective and excitation wavelengths of 488 and 561 nm. N-SIM images were collected on a Nikon Eclipse Ti using a 100x/1.49 CFI Apo TIRF objective using 488 and 561 nm excitation lines. SIM images were collected at 100-200 nm Z-axis steps, with 5-9 rotations of the structured illumination grid were carried out per channel. An iXon 885 EMCCD camera (Andor) was used for acquisition, bearing 8 x 8 μm pixels and a 1004 x 1002 chip resolution. Resulting stacks were processed using default reconstruction parameters in ZEN 2011 software, followed by channel alignment based on measured affine transformation characteristics of the given objective.

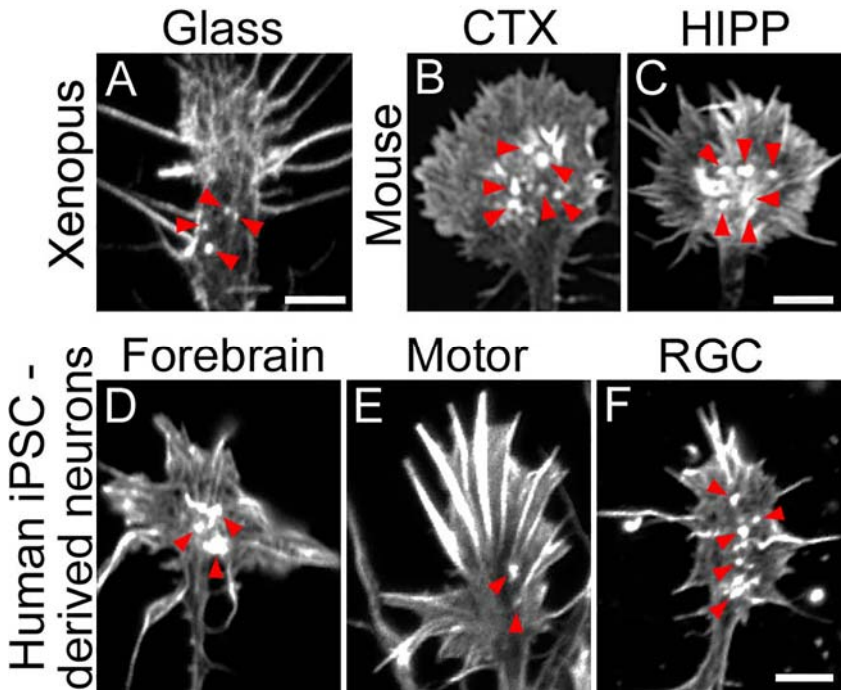

Fig. S1. Mouse and human neuronal growth cones form F-actin rich foci. F-actin in growth cones was labeled with fluorescent phalloidin and imaged by confocal microscopy. **A.** A *Xenopus* spinal neuron growth cone cultured on bare glass. **B-C.** Mouse embryonic cortical (B) and hippocampal (C) growth cones on PDL-L1. **D-F.** Growth cones of human forebrain (D), motor (E) and RGC (F) neurons differentiated from iPSCs and plated on PDL-LN. Note F-actin rich foci located within the C-domain of all growth cones (arrowheads). Scale, 5 μm (A-F).

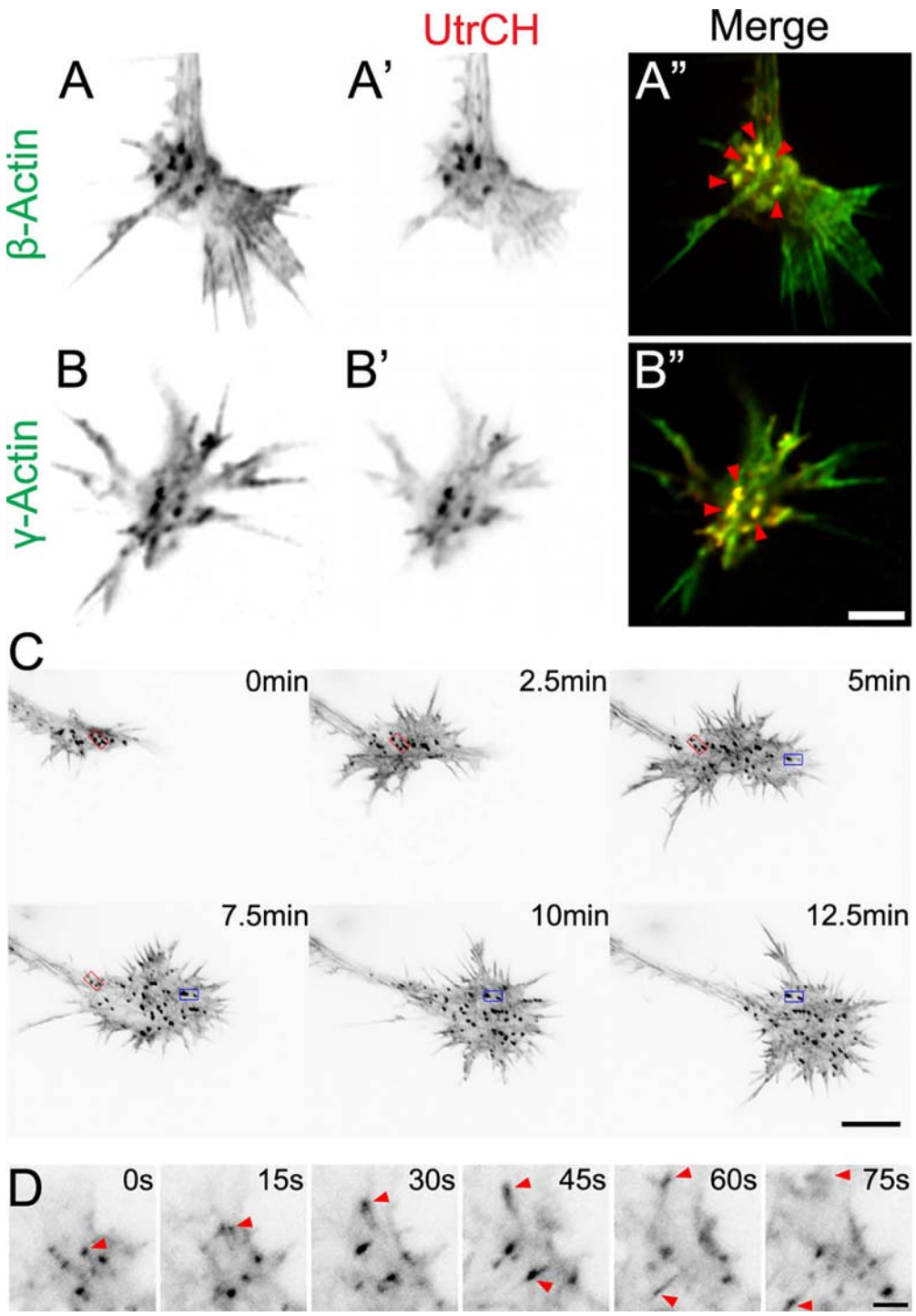

Fig. S2. Both β and γ isoforms of actin target to F-actin rich foci within the C-domain of growth cones. A,B. Live growth cones on LN expressing GFP-β-actin (A) or GFP-γ-actin (B) together with mCh-UtrCH (A', B') imaged by TIRF (inverted contrast). Note in merged images (A", B") that both β-actin

and γ-actin (green) colocalize with mCh-UtrCH (red) labeled F-actin foci (arrowheads). **C.** Time series TIRF images of a live growth cone on LN expressing mCh-UtrCH to label F-actin (inverted contrast). Note that a subset of F-actin foci are highly stable (red and blue boxes). **D**. Time series TIRF images of the leading edge of a growth cone expressing mCh-UtrCH (inverted contrast). Note that some foci appear motile (arrowheads). Scale, 5 μm (A-B), 10 μm (C), 2.5 μm (D).

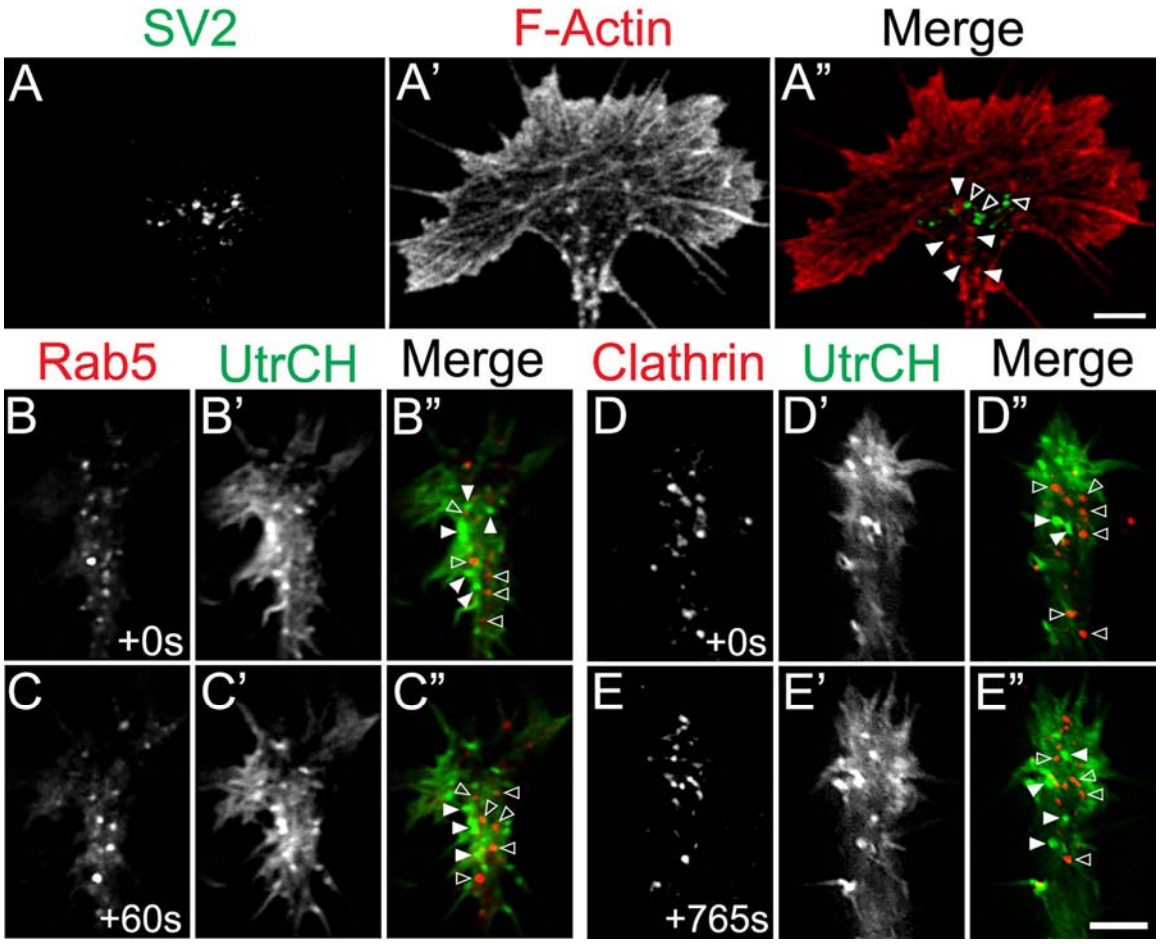

Fig. S3. F-actin foci do not colocalize with exocytotic synaptic vesicles or endocytic vesicles. **A.** Confocal images of a growth cone on LN, immunolabeled for SV2 (A) and F-actin using Alexa-546 phalloidin (A'). **A".** Merged image of SV2 (green) and F-actin (red) shows little colocalization between synaptic vesicles (open arrowheads) and F-actin foci (solid arrowheads). **B-E.** Two time-point TIRF images of live growth cones on LN expressing either mCh-Rab5A (B, C) or DsRed-Clathrin light chain (D, E) and GFP-UtrCH to label F-actin (B'-E'). Note little colocalization between F-actin foci (solid arrowheads, green) and Rab5 or Clathrin (open arrowheads, red). Scale, 5 μm (A-E).

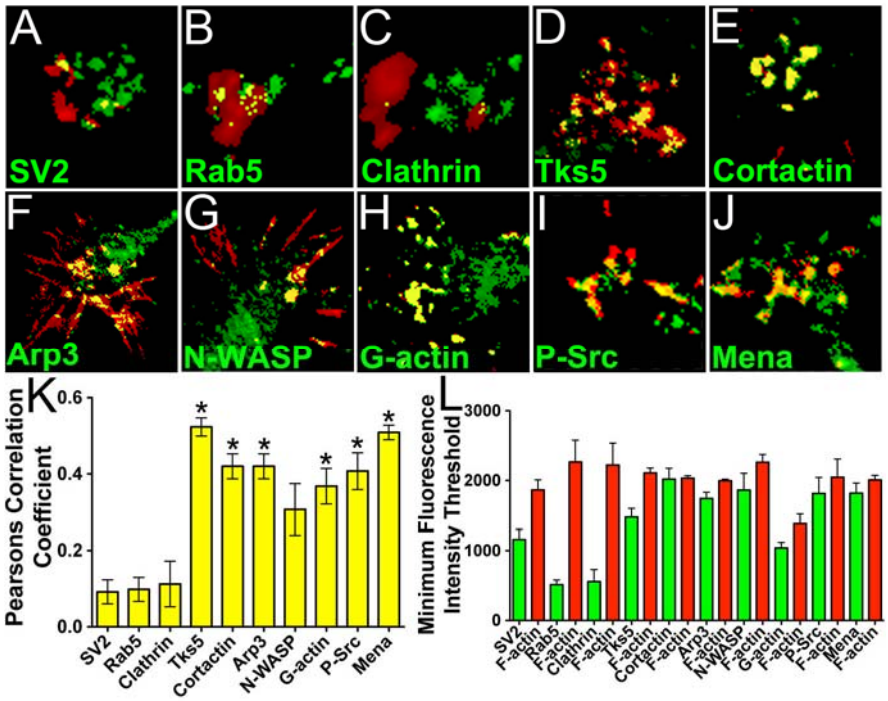

Fig. S4. Quantification of F-actin foci colocalization with various markers by Pearson's correlation coefficient. A-J. Specific protein labeling (green) is merged with F-actin labeling with phalloidin (red) for each image. Fluorescent images were thresholded to highlight foci. Little colocalization with F-actin foci (yellow) is observed with SV2 (A), Rab5 (B) or Clathrin (C). However, Tks5 (D), Cortactin (E), Arp3 (F), N-WASP (G), G-actin (H), pY418-Src (I) and Mena (J) all show robust colocalization at F-actin foci. Note that Rab5 and Clathrin were detected as expressed fluorescent fusion protein-conjugates, whereas G-actin was labeled with fluorescent DNase1, and all other proteins were detected by ICC. **K.** The average Pearson's correlation coefficients show significantly greater colocalization of F-actin foci with invadosomal markers compared to each of the vesicle markers. **L.** The average minimum threshold values used to generate Pearson's correlation coefficients for each labeling were not significantly

different. Note that lower minimum intensity thresholds were necessary for mCh-Rab5 and DsRed-Clathrin, as these expressed proteins were dimmer than immunolabelings. *P < 0.05, invadosomal marker compared to vesicle marker, One-way ANOVA, N ≥ 4 growth cones for each marker.

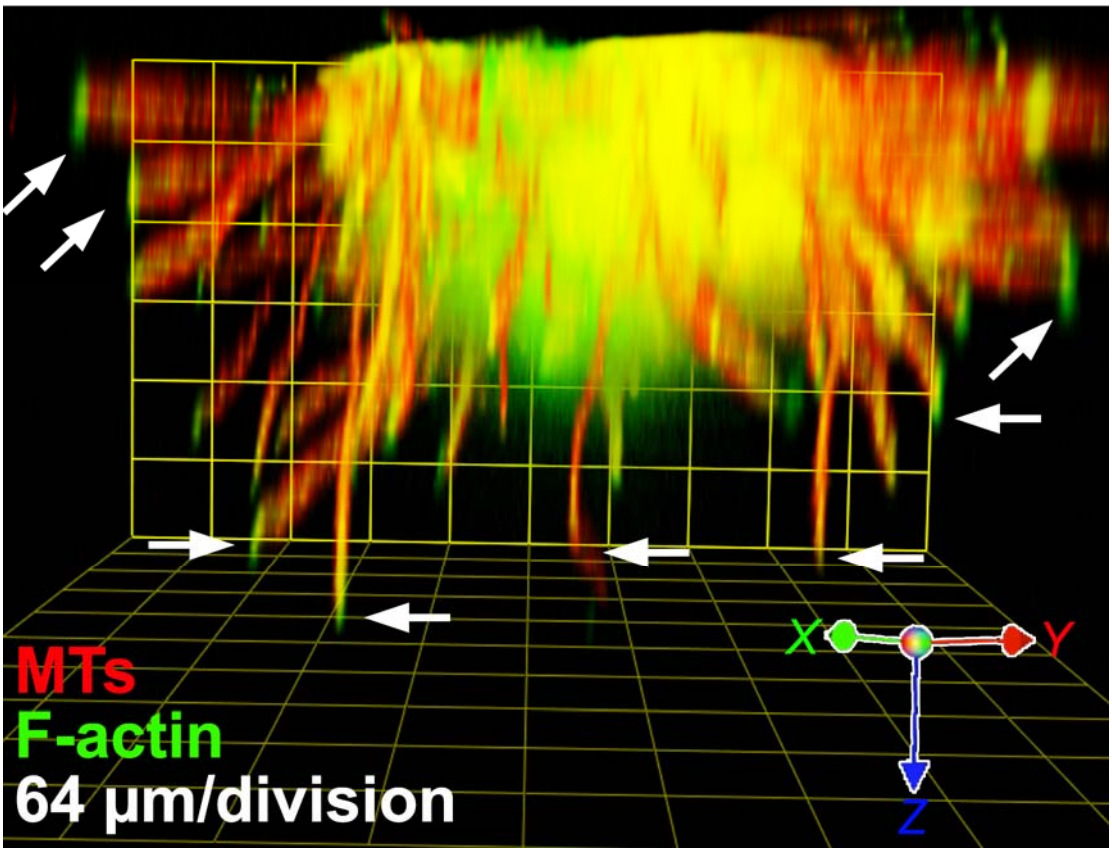

Fig. S5. *Xenopus* spinal axons extend deep into a 3D collagen gel. Confocal Z-series 3D reconstruction of a *Xenopus* spinal explant cultured on top of a collagen-1 gel. The explant was fixed and stained for F-actin with phalloidin (green) and immuolabeled for MTs (red). The deepest axons tipped by growth cones (arrows) extend greater than 300 µm into the gel.

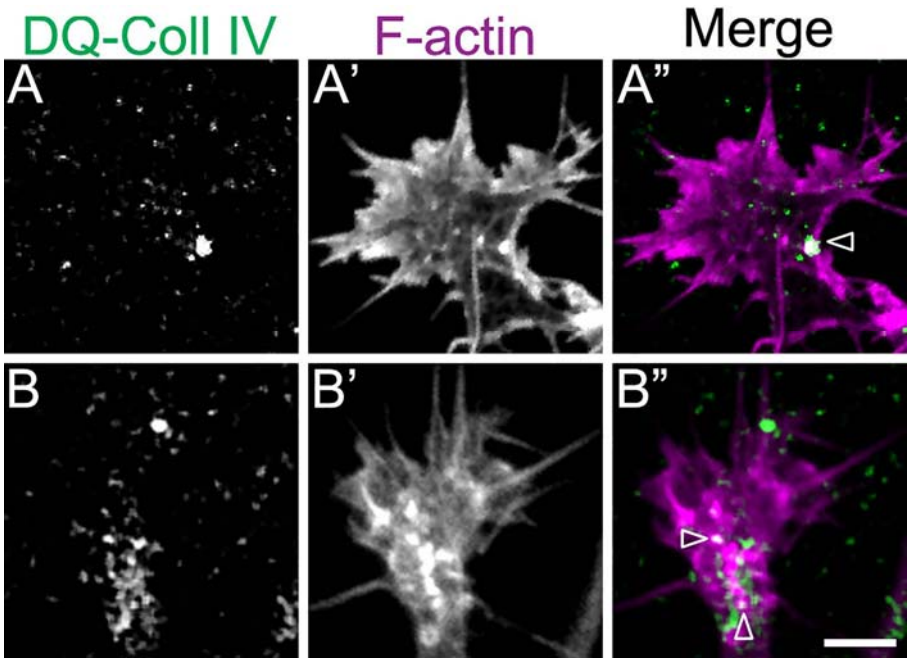

Fig. S6. Growth cone invadosomes are sites of ECM degradation. A, B. Confocal images of spinal growth cones cultured on DQ-collagen IV. **A', B'.** Phalloidin labeling of F-actin. **A", B".** Merged images of the DQ-collagen IV (green) and F-actin label (magenta). Note the colocalization of growth cone invadosomes with areas of collagen degradation visualized as sites of unquenched fluorescence (open arrowheads). Scale, 5 μm (A-B).

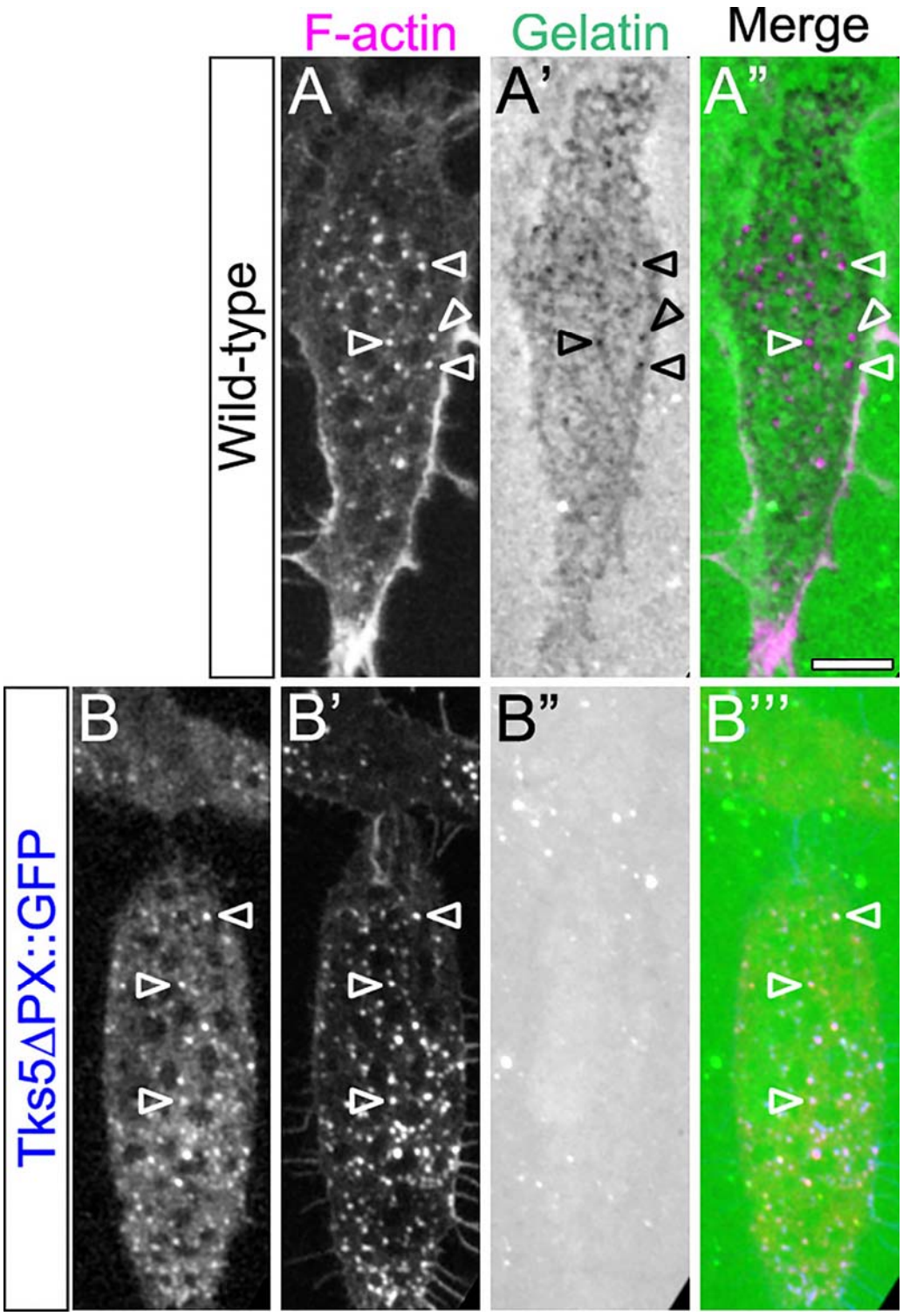

Fig. S7. Dominant negative Tks5, Tks5ΔPX, attenuates gelatin degradation. A-A". Confocal image of a Xenopus neural crest cell on Oregon green 488 gelatin (green in merge), fixed and stained for F-actin (magenta in merge) with Alexa-546 phalloidin. Note the sites of gelatin

degradation under invadosomes in the merge (A”). **B-B’’’.** Confocal image of a Xenopus neural crest cell expressing Tks5ΔPX (B, blue in merge) on Cy3-labeled gelatin (B’, green in merge), fixed and stained for F-actin (B”, red in merge) with Alexa-546 phalloidin. Note the lack of gelatin degradation under invadosomes in the merge (B’’’). Scale, 10μm.

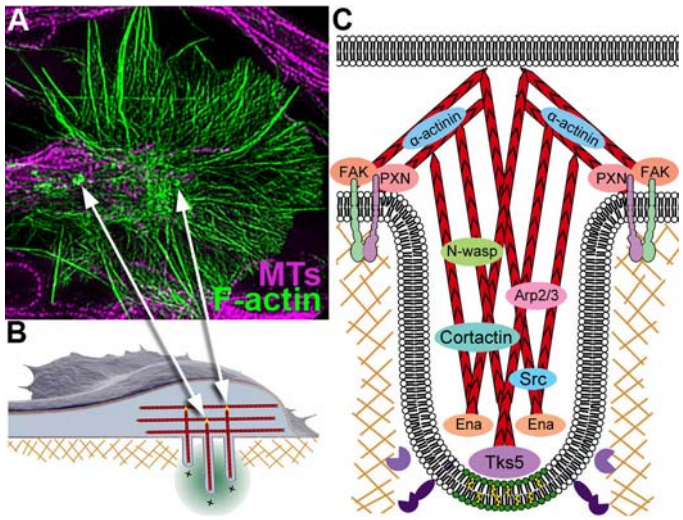

Fig. S8. Model illustrating F-actin rich foci as growth cones invadosomes. **A.** SIM image of a *Xenopus* spinal neuron growth cone on LN, fixed and stained for F-actin (green) with Alexa-568 phalloidin and immunolabeled for βI/II-tubulin (magenta). Note the F-actin rich foci within the growth cone C-domain (arrows). **B.** Illustration of a cross-sectioned growth cone responding to environmental cues by remodeling the ECM with F-actin foci that become protruding invadosomes. Note how invadosomal F-actin orients perpendicular to the planar F-actin network within the growth cone. **C.** Magnified schematic view of a single cross-sectioned growth cone invadosome. Growth cones first establish adhesions with the ECM through the interaction of integrins, Src and adhesion proteins such as paxillin and FAK. Once localized to adhesion sites, Src may phosphorylate Tks5, as well as proteins implicated in lipid raft formation. Phosphorylated Tks5 targets to lipid rafts and initiates actin polymerization through cortactin, N-WASP, the Arp2/3 complex and Ena/Vasp proteins. This network of branched actin assembles F-actin rich columns that span the width of the growth cone and

extend protrusions orthogonal to the plane of outgrowth. Membrane bound and secreted proteases at the tips of invadosomes begin to degrade the ECM, allowing the actin column to transition into a 3-dimensional membrane protrusion. Invadosomal protrusions, formed of both branched and unbranched actin filaments, are stabilized by proteins such as α-actinin. In mature invadosomes, MTs polymerize into the protrusion providing increased stability and the delivery of vesicular cargo, such as proteases and guidance cue receptors. Growth cone invadosomes may represent a novel mechanism for growth cones to respond to environmental cues by remodeling surrounding tissues with 3-dimensional projections during axon guidance.

Movie 1. Growth cones form numerous stable F-actin foci *in vitro* detected by time-lapse GFP-β-actin imaging. Time-lapse TIRF image sequence acquired with a 100X/1.49NA objective of a growth cone on LN expressing GFP-β-actin. This image sequence shows the growth cone from Fig. 1E. Images were captured at 10 sec intervals for 15 min. Playback is 10 frames / sec. Scale bar, 5 µm.

Movie 2. Growth cones form numerous stable F-actin foci *in vitro* detected by time-lapse mCh-UtrCH imaging. Time-lapse TIRF image sequence acquired with a 100X/1.49NA objective of a growth cone on LN expressing mCh-UtrCH, which specifically binds F-actin. This image sequence shows the growth cone from Fig. S2C. Images were captured at 15 sec intervals for 15 min. Playback is 14 frames / sec. Scale bar, 10 µm.

Movie 3. Paxillin targets transiently to F-actin foci. Two channel time-lapse TIRF image sequence acquired with a 100X/1.49NA objective of a growth cone on LN expressing PXN-GFP and mCh-UtrCH. Single channel images are shown as inverse contrast, while merge shows pseudo-colored paxillin (green) and F-actin (red). This image sequence shows the growth cone from Fig. 2E-G. Images were captured at 15 sec intervals for 10 min. Playback is 8 frames / sec. Scale bar, 5 µm.

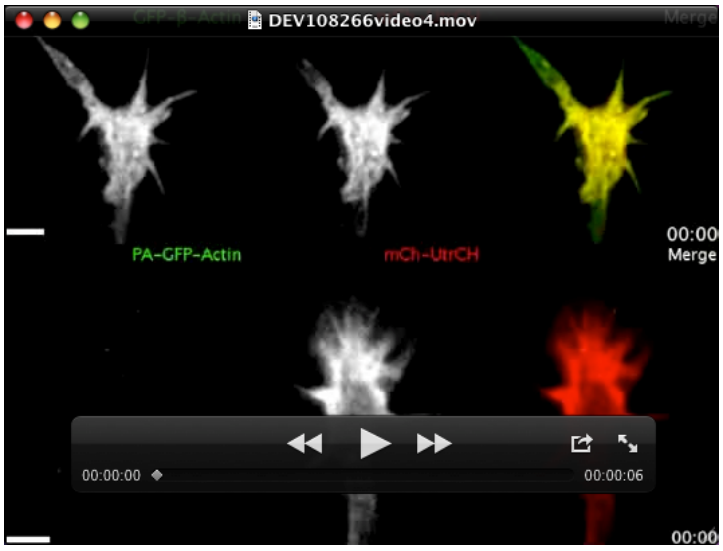

Movie 4. FRAP and FDAP of actin at F-actin foci. Time-lapse confocal image sequence acquired with a 100X/1.45NA objective of growth cones on LN expressing GFP-β-actin and mCh-UtrCH (top) or paGFP-γ-actin and mCh-UtrCH (bottom). This image sequence shows the growth cones from Fig. 3D-F. Images were captured at 1 sec intervals for 64 seconds. Playback is 10 frames/sec. Scale bars, 5 µm.

Movie 5. F-actin foci colocalize with Cortactin. Time-lapse TIRF image sequence acquired with a 100X/1.49NA objective of a growth cone on LN expressing GFP-Cttn and mCh-UtrCH and treated with BDNF. Note Cttn and F-actin colocalize at stable and mobile puncta. Images were captured at 15 sec intervals for 50 min. Playback is 14 frames / sec. Scale bar, 5 µm.

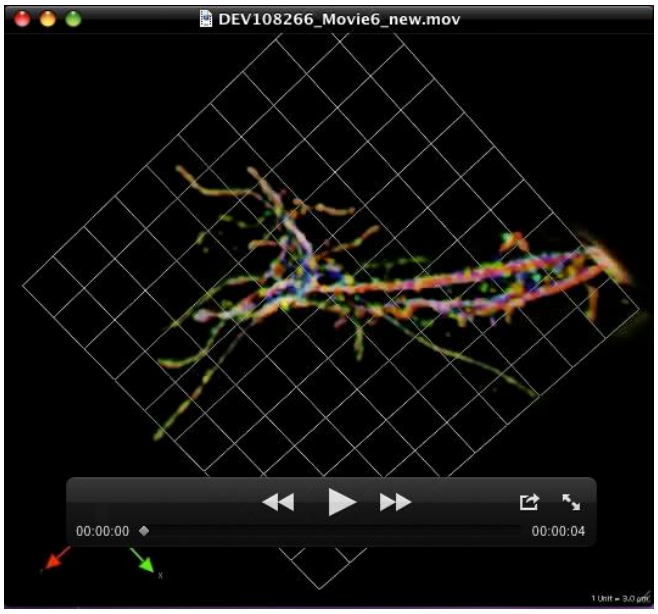

Movie 6. A growth cone in collagen has F-actin foci that are orthogonal protrusions that penetrate into the gel. 3D rotation of a SIM image of a growth cone in a collagen I gel labeled for Cttn (green), MTs (red) and F-actin (blue). Note that Cttn puncta in the central domain of these highly filopodial growth cones are associated with orthogonal protrusions. Image z-series was collected on a Nikon N-SIM microscope. This image sequence shows the growth cone from Fig. 6G.

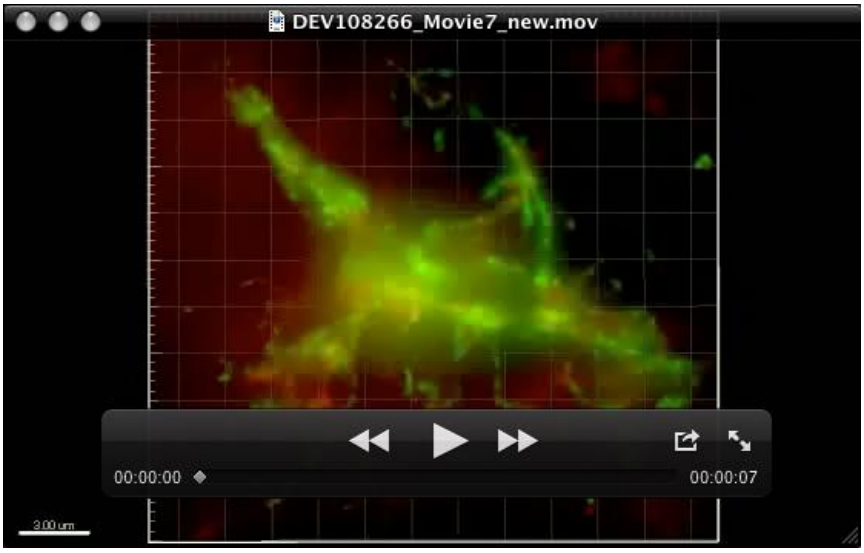

Movie 7. Rohon-Beard growth cones extend invadosome-like protrusions toward the peripheral skin within intact embryos. 3D rotation of a SIM image of a Rohon-Beard growth cone in the peripheral skin of a *Xenopus* embryo labeled for NCAM (Hnk-1, green) and Cttn (red). Note that Cttn puncta near the central domain are associated with orthogonal protrusions that extend toward the skin. Image z-series was collected on a Zeiss ELYRA SIM microscope. This image sequence includes the growth cone depicted in Fig. 7D.

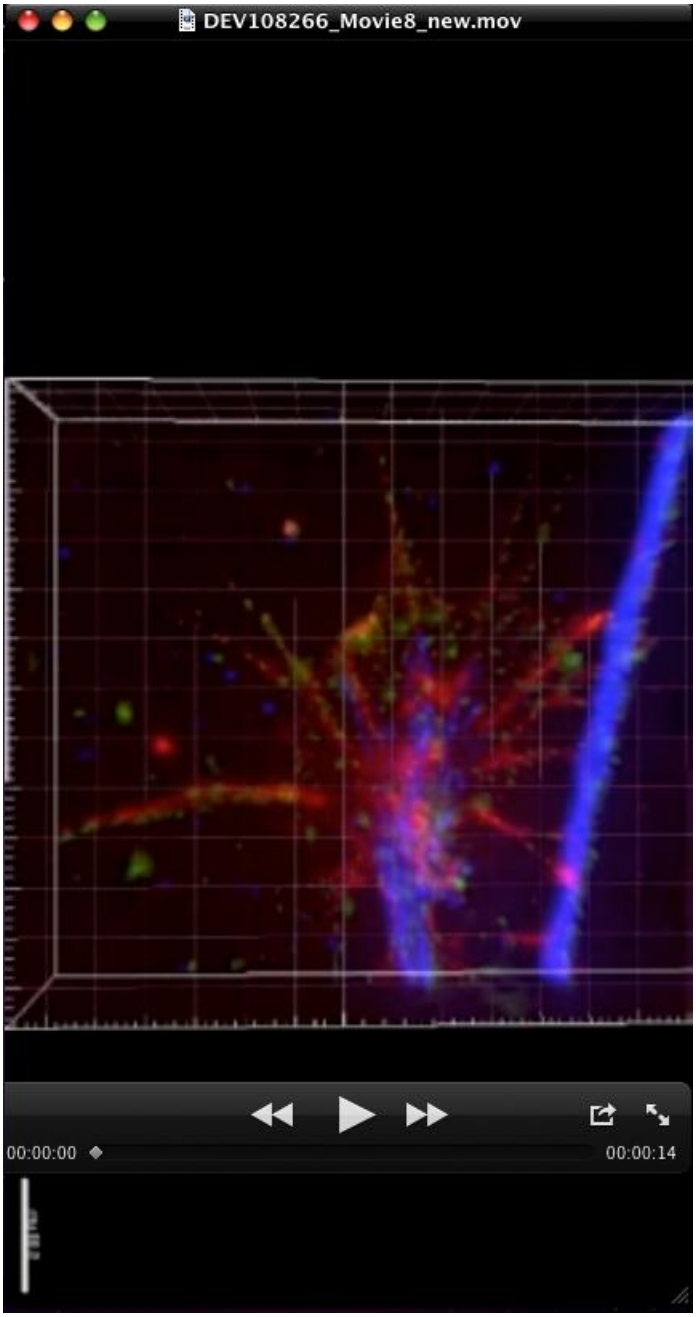

Movie 8. A growth cone with an apical protrusion from the central domain is tipped by ADAM17 MMP. 3D rotation of a super resolution SIM image of a human forebrain neuron growth cone derived from an iPSC on LN immunolabelled for MTs (blue), F-actin (red) and ADAM17 (green). Note that a F-actin foci in the central domain is associated with an apical protrusion that is also ADAM17 positive. Image z-series was collected on a DeltaVision OMX-SIM microscope. This image sequence is the same growth cone shown in Fig. 6E.

Movie 9. GFP-ΔPX-Tks5 clusters into highly mobile puncta within a neural crest cell. Time-lapse TIRF image sequence of a neural crest cell on LN expressing GFP-ΔPX-Tks5. Images were captured at 10 sec intervals for 15 min with a 100x/NA 1.49 objective. Playback is 14 frames / sec. Scale bar, 5 µm.

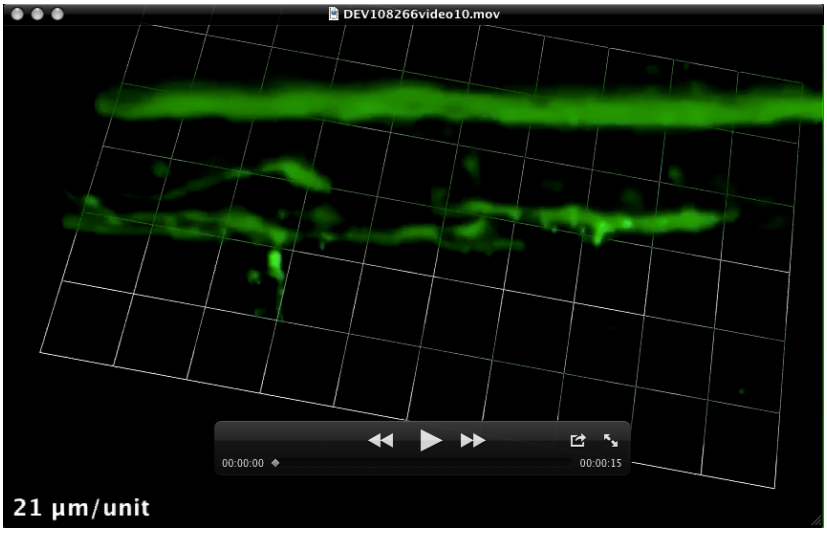

Movie 10. Pioneer MN axons extend invadosome-like protrusions toward the peripheral myotome in vivo. 3D x-axis rotation of a confocal reconstruction of the early spinal cord labeled for synaptotagmin 2 (Znp-1). Note several fine protrusions extend laterally toward the periphery from the terminal of a MN axon on the ventral fascicle.